International Journal of Advanced and Applied Sciences, 13(8) 2026, Pages: 83-107

Contents lists available at Science-Gate

International Journal of Advanced and Applied Sciences

Journal homepage: https://www.science-gate.com/IJAAS.html

Techno-economic and CO_2 impacts of AI-enabled transparent BIPV façades in Saudi smart-city sites: Multi-site simulation

Abdalrahman Alhndawi [1,*], Muhamad Ali Bin Muhammad Yuzir [1], Haneen Nsair [2]

[1]Department of Environmental Engineering, Faculty of Civil Engineering, Universiti Teknologi Malaysia (UTM), Johor Bahru, Johor, Malaysia
[2]Department of Architecture and Urban Planning, College of Engineering, Qatar University, Doha, Qatar

ARTICLE INFO

Article history:
Received 17 February 2026
Received in revised form
26 July 2026
Accepted 14 August 2026

Keywords:
AI-enabled operation
Building-integrated photovoltaics
Net CO_2
Saudi smart cities
Transparent photovoltaics

ABSTRACT

This study evaluates the techno-economic performance and CO_2 benefits of transparent building-integrated photovoltaics (BIPV) façades with AI-enabled operation across four Saudi smart-city sites (NEOM, Riyadh, Red Sea, and AlUla). The objective is to quantify how an AI decision-support layer affects electricity generation, levelized cost of electricity (LCOE), discounted payback, return on investment (ROI), and CO_2 outcomes. A multi-site, per-m^2 façade simulation is conducted at hourly resolution and aggregated into monthly and annual indicators. Three cases are compared: conventional PV (S1), transparent PV without AI (S2), and AI-enabled transparent PV (S3); a maintenance-constrained case (S3b) is also assessed. AI is represented as condition-based loss recovery through reduced soiling-related losses and improved cleaning responsiveness, without altering PV device physics. Results show that S3 improves transparent-façade yield relative to S2 by ≈8.75–9.22%, reducing LCOE by ≈7.4–7.9%, shortening payback by ≈1.2–1.3 years, and increasing ROI by ≈0.8–0.9 percentage points. Avoided operational CO_2 increases proportionally with delivered electricity. Economic realism and probabilistic uncertainty analyses indicate that feasibility depends on tariff and financing conditions, AI/controls cost, and maintenance practicality. Overall, conventional PV should be prioritized for bulk generation, while AI-enabled transparent façades are suitable as a complementary resource where architectural and planning constraints justify façade integration.

1. Introduction

Smart-city growth is increasing electricity use while also increasing the pressure to deliver urban services with lower carbon emissions. Therefore, city planners are placing greater emphasis on integrating renewable energy with digital energy management systems (Ali et al., 2023; Almihat et al., 2022; Kim et al., 2021). Solar photovoltaics remain one of the most practical options for reducing emissions from urban electricity, but installations in cities are often constrained by small roof areas, shading from nearby buildings, and competition for rooftop space (Ang et al., 2022; Izam et al., 2022). Building-integrated photovoltaics (BIPV) helps address these limits by using more of the building's exterior for solar collection, including façades widely available in dense areas and high-rise smart-city designs (Almihat et al., 2022; Hoang and Nguyen, 2021; Kim et al., 2021). In addition, semi-transparent and transparent photovoltaic options are especially suitable for façades and glass surfaces because they can maintain daylight and support building appearance while still generating electricity (Huang and Markides, 2021; Katepalli et al., 2023).

Saudi Arabia is a strong case for façade-based solar, as national transition plans are accelerating renewable-energy expansion alongside major smart-city developments (Al-Saidi, 2022; Islam and Ali, 2024). Smart-city programs that focus on advanced public services, grid upgrades, and sustainability rating systems also increase the value of distributed, building-level generation that can be tracked and improved over time (Ali et al., 2023; Arévalo and Jurado, 2024; Deeb et al., 2024). However, buildings in Saudi Arabia also operate under difficult conditions—very high temperatures, strong sunlight,

* Corresponding Author.
Email Address: dr.adh93@gmail.com (A. Alhndawi)
https://doi.org/10.21833/ijaas.2026.08.009
Corresponding author's ORCID profile:
https://orcid.org/0009-0003-4562-7763

and dust accumulation—which can lower PV output and make façade-level upkeep more challenging (Al-Shetwi, 2022; Ang et al., 2022; Cherupurakal et al., 2021). As a result, it is important to measure not only how much energy transparent BIPV can produce, but also what it means for costs and emissions when deployed across different Saudi smart-city locations (Al-Saidi, 2022; Chen et al., 2021; Islam and Ali, 2024).

Although PV materials and semi-transparent cell designs have advanced rapidly, transparent PV systems often face a clear trade-off between efficiency and visibility, which can widen the performance gap compared with standard opaque modules (Ashraf et al., 2023; Katepalli et al., 2023). Consequently, transparent BIPV façades require careful technical and economic testing to determine whether their design and urban advantages justify a higher cost per kilowatt-hour under real-world climate conditions (Chen et al., 2021; Elia et al., 2021; Hoang and Nguyen, 2021). Losses caused by dust buildup and light reflection are especially significant in dusty regions, which has increased interest in improved surface treatments and self-cleaning solutions; however, these challenges also point to the need for well-planned operation and maintenance strategies (Al-Shetwi, 2022; Ang et al., 2022; Cherupurakal et al., 2021). At the same time, artificial intelligence (AI) is increasingly being used to support renewable-heavy energy systems by improving forecasting, guiding operational decisions, and strengthening asset management across large deployments (Abisoye et al., 2024; Bennagi et al., 2024; Boza and Evgeniou, 2021).

AI approaches are often applied to reduce uncertainty in variable renewable energy output through short-term prediction, to support control actions, and to help schedule maintenance to reduce downtime and limit performance decline (Abisoye et al., 2024; Arévalo and Jurado, 2024; Boza and Evgeniou, 2021). Studies reviewing AI in renewable energy note that benefits usually come less from changing how PV systems operate and more from reducing operational losses and improving decision-making across planning and day-to-day operations (Arévalo and Jurado, 2024; Bennagi et al., 2024). However, many published works separate AI performance results from economic feasibility, creating a need for research that clearly measures how an AI-enabled operations layer changes annual energy output, cost metrics, and emissions savings—particularly for transparent BIPV façades in harsh-climate smart cities (Abisoye et al., 2024; Arévalo and Jurado, 2024; Chen et al., 2021). For Saudi Arabia specifically, there is still limited evidence across multiple sites that compares transparent BIPV performance with and without AI support under the same assumptions and evaluation criteria (Al-Saidi, 2022; Deeb et al., 2024; Islam and Ali, 2024).

This paper responds to that need by presenting a multi-site simulation study of transparent BIPV façades in Saudi smart-city locations, comparing cases with and without AI-enabled operation across three decision layers: energy performance, techno-economics, and operational CO_2 impact. The main goal is to measure how AI-supported operations affect annual energy yield and, in turn, the levelized cost of electricity (LCOE), payback period, and return on investment (ROI). In addition, the study estimates avoided CO_2 emissions using an operational accounting boundary. The work makes six contributions: (1) a consistent multi-site, per-m^2 façade functional-unit comparison across NEOM, Riyadh, the Red Sea Project, and AlUla; (2) an explicit AI-enabled operational logic description (inputs, clean-power estimator, soiling indicator, trigger rules, and false-trigger mitigation) that links condition-based actions to energy-yield recovery; (3) strengthened model credibility through literature-based validation and an additional façade-relevant benchmark; (4) an upgraded robustness assessment that complements OFAT sensitivity with probabilistic (Monte Carlo) uncertainty quantification; (5) expanded environmental reporting by complementing operational avoided CO_2 with a simplified embodied-carbon screening for key BIPV and AI components; and (6) a maintenance-feasibility (access-constrained) scenario to test the sensitivity of S3 benefits to realistic façade cleaning constraints. This study considers AI at the level of overall system effects and does not focus on specific model designs or predictive-maintenance classifiers; instead, it emphasizes how AI enablement changes system-level results.

2. Literature review

2.1. Transparent photovoltaics and transparent BIPV façade systems

Transparent and semi-transparent PV enable solar generation to be integrated into building façades and glazing when conventional opaque modules conflict with architectural appearance, daylighting needs, or façade design constraints. This is particularly relevant in dense smart-city districts, where vertical surfaces can expand on-site generation beyond limited roof area (Hoang and Nguyen, 2021; Kim et al., 2021). A central design constraint is the transparency–efficiency trade-off: increasing visible-light transmission generally reduces electrical conversion, so transparent BIPV assessments must jointly consider optical performance (e.g., VLT/daylighting) and delivered electricity rather than electricity output alone (Huang and Markides, 2021; Katepalli et al., 2023).

Approaches such as spectral management and combined PV/thermal designs demonstrate that semi-transparent devices can serve as useful building-envelope components while, in some cases, improving overall energy use. However, façade-scale deployment continues to face practical hurdles, including strong dependence on orientation, added wiring and compliance requirements, and long-term stability of both optical and electrical performance under real exposure (Ashraf et al., 2023; Gupta et al., 2021; Huang and Markides, 2021; Izam et al., 2022; Katepalli et al., 2023). As a result, transparent BIPV in smart-city design is typically justified as a supporting envelope solution that extends solar harvesting beyond roofs, but only when feasibility evidence clearly addresses yield, cost, and sustained performance over time (Chen et al., 2021).

2.2. Performance determinants in hot-arid and dust-prone environments

In hot-arid regions, high operating temperatures can significantly reduce PV output because higher cell temperatures lower voltage and overall power. In addition, façade integration can alter heat transfer and ventilation compared with rooftop systems, potentially further affecting temperature-related losses (Al-Shetwi, 2022; Ang et al., 2022; Ashraf et al., 2023; Izam et al., 2022). Dust and soiling are also ongoing causes of performance loss in desert conditions because particles reduce light transmission and can increase mismatch losses. For façade systems, cleaning can be more difficult due to limited access and safety requirements, making realistic maintenance assumptions especially important (Al-Shetwi, 2022; Ang et al., 2022).

Material and surface solutions, including superhydrophobic and anti-reflective self-cleaning coatings, have been proposed to reduce soiling losses. However, their long-term reliability under abrasive dust, intense UV exposure, and extended service life remains uncertain for façade-scale applications (Ashraf et al., 2023; Cherupurakal et al., 2021). In addition, vertical installation changes the angle at which sunlight strikes the surface and shifts seasonal irradiance patterns, while dense urban settings add complex shading and reflection effects. Therefore, site-specific modeling is needed to avoid drawing misleading conclusions from horizontal irradiance data alone (Ang et al., 2022; Hoang and Nguyen, 2021; Kim et al., 2021).

2.3. Artificial intelligence as an operational enabler for PV and BIPV systems

Automated, data-driven operation has often been presented as a way to improve renewable system performance through better prediction, operational support, and maintenance analysis. This is especially relevant in smart-city contexts, where sensor networks and digital platforms can track many distributed systems continuously (Ali et al., 2023; Arévalo and Jurado, 2024; Bennagi et al., 2024; Wolniak and Stecuła, 2024). Among these uses, short-term generation prediction is the most established because more accurate forecasts can reduce uncertainty and improve coordination with storage and flexible demand. As a result, the main benefits are usually seen as reduced losses and improved reliability, rather than changes to how modules convert sunlight into electricity (Abisoye et al., 2024; Bennagi et al., 2024; Boza and Evgeniou, 2021).

In addition, automated fault identification and maintenance prioritization can limit downtime and target corrective actions, which matters in harsh climates where soiling and other stressors can cause frequent deviations that are difficult to handle through manual inspection alone (Al-Shetwi, 2022; Bennagi et al., 2024; Zhang et al., 2022). However, results do not always transfer cleanly from one site to another because performance depends on data availability, sensor quality, and local operating conditions. Therefore, comparisons across locations require clear assumptions and consistent evaluation methods (Abisoye et al., 2024; Arévalo and Jurado, 2024; Chen et al., 2021). More broadly, system-level studies of smart grids and microgrids also describe these tools as supporting resilience and loss reduction in electricity networks with high renewable shares (Konstantinou, 2021).

2.4. Techno-economic assessment frameworks for PV and BIPV

Techno-economic assessments typically separate upfront costs (CAPEX) from ongoing costs (OPEX) over a defined lifetime and commonly report LCOE, payback period, and ROI. However, BIPV evaluations require careful boundary choices because integration costs and the extent to which PV replaces conventional building-envelope elements are not consistently allocated across studies (Ang et al., 2022; Chen et al., 2021; Hoang and Nguyen, 2021). When assumptions are clearly stated, LCOE helps compare different technologies, while payback and ROI provide decision-friendly indicators. Even so, both can change substantially depending on tariffs, discounting choices, and financing assumptions (Alafnan, 2024; Chen et al., 2021).

Comparisons are often weakened by inconsistent reporting of key inputs, such as the discount rate, degradation, replacement events, and the assignment of façade-integration costs. As a result, headline metrics can be harder to interpret for smart-city planning and procurement (Ali et al., 2023; Almihat et al., 2022; Ang et al., 2022; Chen et al., 2021). In addition, because costs can fall as products mature, scenario-based evaluations can be useful for emerging BIPV options, but only when the underlying assumptions are explicitly stated and consistently applied (Elia et al., 2021; Izam et al., 2022).

2.5. Environmental impact reporting for building-integrated solar

Operational avoided CO_2 is often estimated by multiplying delivered electricity by a grid-emission factor within a clearly defined displacement boundary. When the emission-factor source and boundaries are documented, this method supports consistent comparisons across systems and locations (Al-Shetwi, 2022; Chenic et al., 2022). However, avoided-emissions estimates can vary widely depending on whether average or marginal emission factors are used and whether future grid decarbonization is accounted for. Therefore, transparent assumptions are essential for credible comparisons between technologies and sites (Chenic et al., 2022).

Life-cycle assessment expands the boundary beyond operation to include embodied impacts and allocation rules. This is especially important for BIPV because PV elements may interact with conventional façade materials and construction choices. However, uncertainty in manufacturing scale and long-term durability can make comparisons more difficult for newer PV options (Al-Shetwi, 2022; Chenic et al., 2022; Elia et al., 2021). In the Saudi transition and smart-city setting, decision-focused reporting needs measures that can be compared across projects and communicated clearly, which reinforces the importance of consistent operational CO_2 reporting and well-defined boundaries (Al-Saidi, 2022; Ali et al., 2023; Deeb et al., 2024; Islam and Ali, 2024).

2.6. Synthesis of prior work and identification of research gaps

Across the literature, several themes recur. Smart-city energy planning benefits from distributed renewables and coordinated digital management, and BIPV expands usable PV collection area beyond rooftops by activating building envelopes in dense districts (Ali et al., 2023; Almihat et al., 2022; Kim et al., 2021). In hot-arid environments, PV performance is further constrained by high operating temperatures and soiling, which increases the importance of maintenance planning and performance monitoring for reliable operation (Al-Shetwi, 2022; Ang et al., 2022; Cherupurakal et al., 2021). Prior work also shows that transparent and semi-transparent PV can be integrated into façades and glazing to support daylighting and architectural objectives; therefore, its value is often linked to where conventional PV placement is limited by design or land-use constraints (Huang and Markides, 2021; Katepalli et al., 2023).

In parallel, research on AI and data-driven operations indicates that forecasting, anomaly detection, and maintenance-focused analytics can reduce avoidable losses and strengthen the resilience of renewable systems (Abisoye et al., 2024; Arévalo and Jurado, 2024; Bennagi et al., 2024; Boza and Evgeniou, 2021). However, most studies either report AI performance improvements without linking them to façade-normalized economic decision metrics or evaluate techno-economic outcomes without explicitly modeling an operational AI layer. As a result, there remains limited evidence that quantifies—under consistent functional-unit and boundary assumptions and across multiple locations—how an AI-enabled operational layer changes façade-specific outcomes such as annual energy yield, LCOE, discounted payback, ROI, and operational avoided CO_2 for transparent BIPV applications (Chen et al., 2021; Wolniak and Stecuła, 2024; Zhang et al., 2022).

A consistent multi-site evaluation remains limited for Saudi smart-city locations that quantifies—using the same functional unit and accounting boundaries—the incremental impact of an AI-enabled operational layer (e.g., condition-based soiling response and maintenance decision support) on energy yield, techno-economic indicators, and operational avoided CO_2 for transparent BIPV façades operating under hot-arid and dust-prone conditions (Al-Saidi, 2022; Arévalo and Jurado, 2024; Chen et al., 2021; Deeb et al., 2024; Islam and Ali, 2024). In addition, the literature provides limited façade-scale validation evidence, frequently relies on operational-only CO_2 boundaries without embodied-carbon screening, rarely quantifies probabilistic uncertainty (beyond deterministic sensitivity), and often omits maintenance-feasibility constraints that can limit achievable cleaning/response intervals for high-rise façades.

3. Methodology

3.1. Study design and scenario definition

This study applies a comparative, multi-site simulation design to evaluate transparent BIPV façade performance under Saudi conditions and to quantify the incremental value of an AI-supported operational approach. Three standardized scenarios were defined to separate technology configuration from operational strategy while maintaining the same functional unit and evaluation boundary across all sites.

Scenario S1 (Traditional PV) serves as the conventional PV reference case for interpreting façade-based transparent PV outcomes. Scenario S2 (Transparent PV without AI) represents a transparent PV façade operated under periodic, schedule-based O&M without algorithmic support. Scenario S3 (AI-enabled Transparent PV) uses the same transparent PV façade configuration as S2 but adds an operational decision-support layer intended to reduce avoidable losses through forecast-informed monitoring, condition-based interventions, and maintenance prioritization, without altering PV device physics (Abisoye et al., 2024; Arévalo and Jurado, 2024; Bennagi et al., 2024). To reflect practical high-rise maintenance constraints, an additional scenario is introduced: Scenario S3b (Maintenance-constrained AI-enabled Transparent PV), which applies the same TPV configuration and AI decision logic as S3 but imposes an operational feasibility constraint (e.g., a minimum achievable cleaning interval and/or delayed work-order execution due to façade-access limitations at height).

System performance is estimated through a simulation workflow linking site meteorological data to PV/TPV performance modeling and then to system-level indicators (Ang et al., 2022; Izam et al., 2022). Outputs are computed at an hourly time step and aggregated to monthly and annual values to obtain delivered electricity. Annual electricity outcomes are then translated into techno-economic indicators (LCOE, discounted payback period, and ROI) using life-cycle costing assumptions (Chen et al., 2021; Elia et al., 2021). Environmental outcomes are reported as operational CO_2 avoidance by multiplying delivered electricity by an assumed grid emission factor under a clearly defined displacement boundary (Chenic et al., 2022). This consistent scenario structure and aggregation method enable fair cross-site comparison of energy, economic, and operational CO_2 impacts (Ang et al., 2022; Chen et al., 2021).

3.2. Case-study sites and site-specific parameterization

The assessment covered four Saudi smart-city locations—NEOM, Riyadh, the Red Sea Project, and AlUla—to represent different development contexts and to test whether operational support benefits remained consistent under varied climatic conditions (Al-Saidi, 2022; Deeb et al., 2024; Islam and Ali, 2024). This selection included inland hot-arid settings as well as coastal-influenced environments, where PV performance drivers can differ because of temperature patterns and airborne particles (Al-Shetwi, 2022; Ang et al., 2022).

Each site used long-term weather inputs and the same system assumptions, so differences in results were mainly due to location, not to changing methods between sites (Ang et al., 2022; Chen et al., 2021). Temperature-related performance reduction was included because higher operating temperatures reduce PV efficiency and are a major influence on annual yield in hot-arid climates (Ashraf et al., 2023; Izam et al., 2022). Soiling effects were also included because dust buildup reduces light transmission and makes cleaning and maintenance more important, especially for façades where limited access can affect practicality (Al-Shetwi, 2022; Cherupurakal et al., 2021). Façade orientation and sunlight angle effects were considered because vertical or near-vertical systems capture sunlight differently than optimally tilted rooftop PV systems (Ang et al., 2022; Hoang and Nguyen, 2021). Reliability and degradation were handled through life-cycle assumptions, since harsh exposure can speed up performance decline and influence long-term economic outcomes (Ashraf et al., 2023; Chen et al., 2021). A consistent boundary was used for both economic and CO_2 calculations across all sites to support fair cross-site comparisons for smart-city decisions (Chen et al., 2021; Chenic et al., 2022; Deeb et al., 2024).

3.3. Transparent BIPV façade system definition (per m^2 of façade area)

The transparent BIPV façade is defined using a functional unit of 1 m^2 of vertical building-envelope area to ensure consistent cross-site comparison. The system comprises a glazing-integrated transparent PV (TPV) element that generates electricity while transmitting visible light to support daylighting and architectural requirements, consistent with reported use cases for curtain-wall and glazing integration where rooftop PV area is limited (Katepalli et al., 2023).

For all sites, the TPV surface is modeled as a vertical plane (tilt = 90°) with a south-facing orientation (azimuth = 180°) to maintain consistent geometry and to represent a typical high-rise façade configuration. The TPV element is treated as part of an insulated glazing unit (IGU) assembly, with electricity collected via an edge-sealed junction connection to building DC wiring and converted to AC power through an inverter.

The system boundary includes façade-level electricity generation and conversion to AC power and explicitly accounts for major loss mechanisms relevant to Saudi hot-arid operation, including temperature-related derating, soiling losses, inverter and wiring losses, and long-term degradation. Transparent PV is parameterized through its assumed optical–electrical design constraints (visible-light transmission and lower STC efficiency relative to opaque PV), with the adopted performance parameters reported in Table 1 (Huang and Markides, 2021).

Table 1: System technical parameters used for the façade PV configurations (per m^2 basis)

Parameter	Symbol	Unit	S1: Traditional PV (benchmark)	S2/S3: Transparent PV façade (TPV)
Reference façade area	A	m^2	1.0	1.0
Tilt	β	°	90	90
Azimuth (south-facing)	γ_az	°	180	180
Visible light transmittance	VLT	%	0	30
STC module efficiency	η_STC	%	22	8
STC power density (per m^2)	P_STC	W/m^2	220	80
Inverter efficiency	η_inv	%	97	97
DC wiring + mismatch losses	L_dc	%	3	3
Temperature coefficient	μ_P	%/°C	−0.35	−0.30
Nominal operating cell temperature	NOCT	°C	45	48
Annual degradation rate	d	%/year	0.6	0.8
Baseline soiling loss (average)	L_soil	%	5	8
Cleaning interval (periodic baseline)	CI	days	30	30
Service life for accounting	N	years	25	25

3.4. AI enablement description

In this study, AI enablement is described as an operational support layer that improves electricity generation by reducing avoidable losses, especially those caused by soiling. This improvement comes from detecting performance changes earlier and carrying out maintenance actions more quickly.

Therefore, the aim is not to alter how photovoltaic systems physically operate, but to enhance operation and maintenance decisions using standard monitoring data (Deceglie et al., 2018; Sepúlveda-Oviedo et al., 2023). The workflow, shown in Fig. 1, starts by collecting key inputs, including irradiance (or a proxy), temperature, AC power, rainfall data, and system status signals. After filtering the data for quality, the system estimates the expected "clean" power output under the same environmental conditions. It then compares actual and expected outputs to calculate a performance indicator that helps detect possible soiling-related losses. This indicator is evaluated using decision rules that include thresholds, temporal persistence, and event screening to reduce false alarms.

As a result, actions such as cleaning or maintenance alerts are triggered, followed by verification of system recovery and updates to the baseline model.

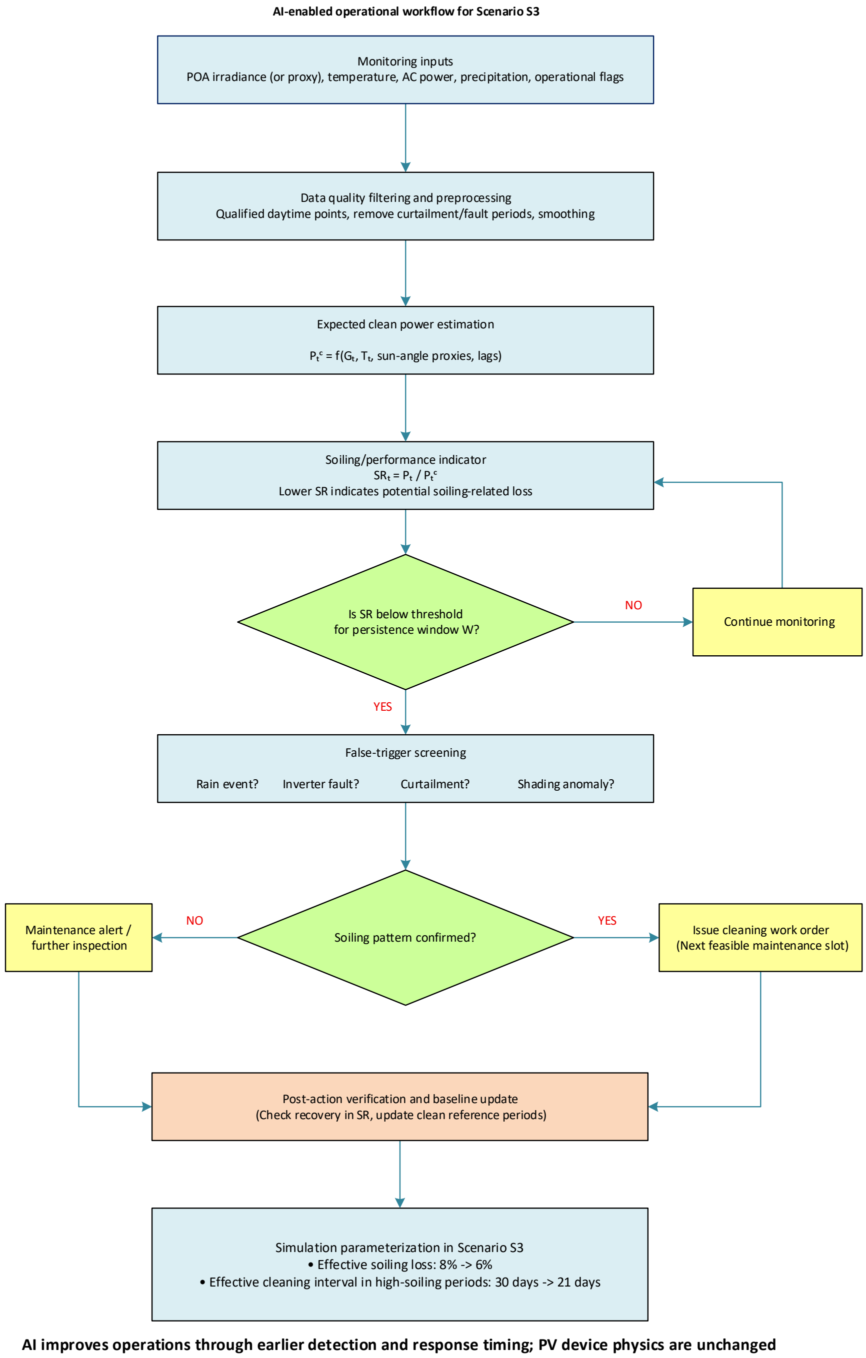

Fig. 1: AI-enabled operational workflow (scenario S3)

3.4.1. Data inputs and sensing layer

The AI layer relies on a standard BIPV monitoring setup suitable for smart-city applications and does not require dedicated soiling sensors. It uses several common inputs, including plane-of-array irradiance (POA), which may be measured directly or estimated from weather data. It also incorporates module or back-surface temperature, or a modeled relationship between ambient and module temperature. In addition, AC power output and inverter status signals are used to track system performance.

Rainfall data help identify natural cleaning events, while operational flags such as curtailment or faults help exclude unrelated performance losses. These data sources are typical in PV/BIPV systems and are sufficient to estimate soiling losses by comparing expected and measured output (Deceglie et al., 2018; Kalimeris et al., 2023). Table 2 clearly presents the assumed inputs and how they are used in the workflow.

Table 2: AI layer assumed inputs, indicators, and triggers

Variable	Source (assumed)	Purpose	How used in workflow
POA irradiance (or proxy)	Pyranometer/reference cell/met-data proxy	Estimate expected clean power	Input for expected output calculation and daytime filtering
Module/back-surface temperature	Sensor or model	Capture temperature effects	Used in estimating expected power under current conditions
AC power Pt	Inverter measurement	Measure actual output	Compared with the expected power to assess performance
Rain/precipitation flag	Weather data	Detect natural cleaning	Identifies clean periods and excludes rainfall events
Inverter status/fault flags	Inverter logs	Remove non-soiling effects	Filters out fault or curtailed operation
Curtailment/clipping flag	Controller/inverter	Prevent misclassification	Avoids false identification of soiling
Sun-angle proxy/time variables	Solar geometry	Improve model accuracy	Supports estimation and filtering
Trigger threshold SRth	Operator-defined	Detect performance drop	Initiates further checks when exceeded
Persistence window W	Operator-defined	Reduce noise	Requires sustained deviation before action
Minimum cleaning interval CImin	O&M constraint	Ensure feasibility	Limits cleaning frequency and supports scheduling

3.4.2. Clean-power estimator (expected output model)

The system calculates expected clean power at each time step using models trained on periods assumed to be clean, such as after rainfall or confirmed cleaning. These models use inputs such as irradiance, temperature, and sun position and can be implemented using established forecasting approaches, including regression-based methods (Antonanzas et al., 2016). The result is an expected clean-power value, denoted as P_t^*, which depends on environmental conditions. This estimate is updated regularly using newly identified clean periods. In this way, the method improves decision-making by refining performance expectations under consistent physical conditions, rather than altering the PV system's underlying operation.

3.4.3. Soiling indicator and decision rules

Soiling is evaluated by comparing measured power with expected clean power through a ratio. A lower ratio indicates reduced performance, which may be linked to soiling after proper data filtering. This indicator is defined as $SR_t = P_t / P_t^*$. However, to avoid reacting to short-term fluctuations, the system uses a two-step decision process. First, the ratio must fall below a defined threshold ($SR_t < SR_{th}$). Second, this condition must persist for a specified time window W. Only when both conditions are satisfied does the system proceed to further checks and possible actions.

3.4.4. False-trigger mitigation and operational constraints

To improve reliability, the workflow includes a screening step that removes events caused by factors other than soiling, such as faults, shading, curtailment, or rainfall. In addition, maintenance alerts are generated when performance patterns deviate from typical soiling behavior, for example, due to sudden drops or when performance does not recover after cleaning. Previous studies highlight the importance of such data-driven monitoring for improving fault detection and reducing downtime (Sepúlveda-Oviedo et al., 2023).

These safeguards are treated as essential operational features in this study. Potential soiling events are excluded if they occur alongside rainfall, faults, curtailment, or detectable anomalies. At the same time, practical maintenance limits are considered. These include a minimum interval between cleaning actions (CI_{min}), scheduling tasks through a work-order queue instead of immediate execution, and escalating to inspection when patterns indicate faults rather than gradual soiling, such as sudden drops or lack of recovery after cleaning.

3.4.5. How AI is represented in the simulation

In the simulation, the role of AI is represented using simplified parameters that reflect improved operational outcomes. Scenario S2 assumes an average annual soiling loss of 8% with cleaning every 30 days, while Scenario S3 assumes a lower loss of 6% and a shorter cleaning interval of 21 days during high-soiling periods. These values reflect the benefits of earlier detection and faster response. However, they are treated as assumed outcomes rather than guaranteed results, and the PV system's physical characteristics remain the same across scenarios. To avoid overstating the role of AI, these values are presented as outcomes consistent with the workflow logic, rather than as measured performance metrics such as accuracy or error rates, which would require large-scale field validation. Finally, uncertainty is addressed through sensitivity analysis, which varies key factors such as implementation costs and soiling reduction. In addition, the maintenance-constrained scenario (S3b) represents situations where maintenance cannot be carried out promptly due to façade access limitations. This provides a conservative estimate of achievable improvements under realistic high-rise maintenance conditions.

3.5. Simulation setup (tools, temporal resolution, and output aggregation)

The study followed a simulation-based workflow that used site weather data to estimate hourly electrical output from PV/TPV systems and then converted those results into monthly and annual key performance indicators (KPIs). This structure helped ensure fair comparisons across locations that experience different hot-arid and dust-prone conditions (Ang et al., 2022; Izam et al., 2022).

Weather time-series inputs were handled at a 1-hour time step. The hourly results were aggregated into monthly totals, then into annual totals to calculate energy yield (kWh/m^2/year). These annual values were used as consistent inputs for the techno-economic calculations. To make the energy-to-cost link clearer and easier to interpret, the simulations explicitly accounted for the main loss sources that affect PV performance in harsh environments, including temperature-related losses, soiling, inverter and wiring losses, and long-term degradation (Al-Shetwi, 2022; Cherupurakal et al., 2021). Table 3 illustrates the simulation configuration settings.

Table 3: Simulation configuration

Item	Setting (complete values)
Simulation time step	1 hour
Simulation horizon	1 typical meteorological year (TMY-equivalent) repeated for lifetime cashflow modeling
Sites	NEOM, Riyadh, Red Sea Project, AlUla
Meteorological sources	SolarGIS (GHI/DNI/DHI), national meteorological station statistics for temperature and humidity, project-specific dust/soiling proxies (all harmonized to hourly series)
PV/TPV performance model	Single-diode equivalent model with temperature derating and loss accounting; inverter conversion applied to obtain AC energy
Losses considered	Temperature derating, soiling, inverter losses, DC wiring/mismatch, availability (downtime), long-term degradation
Soiling representation	Average monthly soiling loss profile with baseline annual mean of 8% for TPV; condition-based reduction applied only in S3 (see Section 3.4)
Performance ratio (PR) approach	PR reported as $PR = \frac{E_{AC}}{H_{POA} \cdot A \cdot \eta_{STC}}$, using plane-of-array irradiance H_{POA}
Primary output variables (hourly)	POA irradiance, module temperature, DC power, AC power, loss components
Aggregated outputs (monthly/annual)	AC energy (kWh/m^2), PR, capacity factor, energy yield uplift (S3 vs. S2), inputs to LCOE/payback/ROI calculations

3.5.1. Model credibility and literature-based validation (sanity checks)

Because this study is based on simulation, a focused validation step was carried out using published literature. The aim is to confirm that the assumed annual PV yield and soiling-loss values are reasonable for hot-arid conditions in Saudi Arabia. In addition, a façade-specific benchmark is included in Section 3.5.2 to strengthen confidence in the assumptions used for vertical BIPV systems. The main validation elements, supporting studies, and comparison outcomes are summarized in Table 4.

For the reference PV yield in Scenario S1, the annual values were compared with monitored data from a large PV system installed on a building (BAPV). Alazazmeh et al. (2022) analyzed a 425 kW system and reported a specific yield of about 1,917 kWh/kWp·yr. When the Scenario S1 results, which range from 1,795 to 1,904 kWh/kWp·yr, are expressed on the same basis, they differ by approximately −6.36% to −0.67%. Therefore, the modeled energy output is consistent with measured performance under Saudi hot-arid conditions.

For the soiling-loss assumptions in Scenarios S2 and S3, the study uses an average annual loss of 8% for transparent PV in S2 and a reduced value of 6% in the AI-enabled S3. These assumptions were checked against field evidence from Saudi Arabia, which shows that soiling losses vary widely depending on location, exposure duration, and cleaning practices. For example, a study in Rumah reported that soiling losses in the literature can range from about 3% to 40%, depending on how they are defined (Baras et al., 2016). In addition, a broader Saudi review reported ranges from 2% to 50% under different environmental conditions (Al Garni, 2022). Therefore, the 8% value can be considered a moderate baseline, while the 6% value reflects a reasonable improvement linked to more responsive maintenance (Al Garni, 2022; Baras et al., 2016).

3.5.2. Additional validation benchmark (façade-relevant evidence)

To further strengthen validation, a façade-specific benchmark based on field data was included. Mohamed et al. (2026) monitored a full-scale vertical BIPV façade system (87.75 kWp) installed on a south-facing wall in Aswan, Egypt, under harsh hot-arid conditions. The study reported that high summer temperatures caused an average power loss of about 8% when the PV operating temperature reached approximately 47°C. Using the same linear temperature-derating method applied in this study (Section 3.3 / Table 1), and assuming a typical coefficient of −0.35%/°C, the predicted loss is (47 − 25) × 0.35% ≈ 7.7%. This differs from the observed value by only about 0.3 percentage points, or roughly 3.8% in relative terms. This close agreement supports the reliability of the temperature-loss assumptions used in the façade simulations, although the results remain scenario-based and do not replace detailed site measurements (Mohamed et al., 2026).

Overall, these validation steps support the credibility of the model results. However, even with the inclusion of façade-specific benchmarking, they do not replace direct validation using measured data from actual façade installations. Future studies should therefore focus on validating vertical BIPV and transparent façade systems using real monitored data, particularly where limited cleaning access may influence performance.

Table 4: Literature-based validation/sanity-check comparison (field evidence vs. this study)

Validation target	This study (where used)	Field evidence (Saudi/hot-arid/façade-relevant)	Agreement statement
Reference PV annual yield magnitude	Scenario S1 annual yield	Monitored 425 kW Saudi BAPV system (Alazazmeh et al., 2022)	Results align within −6.36% to −0.67% of the measured reference on a comparable basis
Soiling-loss magnitude (baseline and improved)	Transparent PV: 8% (S2); improved: 6% (S3)	Saudi studies and reviews (Al Garni, 2022; Baras et al., 2016)	8% fits within reported ranges; 6% reflects moderate improvement from better maintenance
Façade-relevant temperature-derating magnitude	Temperature-loss assumptions in façade simulations	Field-monitored vertical BIPV façade in Aswan (Mohamed et al., 2026)	Predicted ≈7.7% vs. observed ≈8%, showing close agreement and supporting model assumptions

3.6. Techno-economic model

3.6.1. Cost structure and assumptions (CAPEX, OPEX, AI premium, replacements)

The techno-economic analysis followed a life-cycle costing approach that separates the initial investment (CAPEX), ongoing annual costs (OPEX), and replacement expenses incurred over the project lifetime. This format matches common practice for assessing renewable-energy and energy-efficiency options (Chen et al., 2021; Elia et al., 2021).

All costs were expressed per square meter of façade to stay consistent with the functional unit used in the energy simulations. Differences between scenarios were reflected in the cost inputs: S1 used standard assumptions for conventional PV; S2 accounted for the additional costs of integrating TPV into the façade; and S3 included an extra premium for AI/controls, along with a small increase in OPEX to reflect enhanced monitoring and condition-based actions. In this setup, AI-related costs were treated as an operational support layer that affects performance through how the system is run, not through changes to the PV device itself (Bennagi et al., 2024; Chen et al., 2021). Table 5 illustrates the economic assumptions and cost inputs (per m^2).

Table 5: Economic assumptions and cost inputs (per m^2)

Parameter	Unit	S1: Traditional PV	S2: Transparent PV	S3: AI-enabled transparent PV
TPV/PV module + mounting/glazing package	USD/m^2	180	420	420
BIPV façade integration (frames, seals, wiring interface)	USD/m^2	60	180	180
Inverter and power electronics allocation	USD/m^2	35	35	35
Installation & commissioning	USD/m^2	55	70	70
AI/controls premium (sensors, gateway, analytics)	USD/m^2	0	0	35
Total CAPEX (at year 0)	USD/m^2	330	705	740
Annual OPEX (routine O&M + cleaning)	% of CAPEX/year	1.5%	2.0%	2.2%
Inverter replacement	year + % of inverter cost	Year 13; 100%	Year 13; 100%	Year 13; 100%
Controls refresh (software/hardware)	year + % of AI cost	–	–	Year 10; 40%
Project lifetime	years	25	25	25
Real discount rate	%	6.0	6.0	6.0
Electricity value (used for payback/ROI)	USD/kWh	0.07	0.07	0.07

3.6.2. KPI definitions

The levelized cost of electricity (LCOE) represents the average cost of generating one kilowatt-hour of electricity over the system's lifetime, while accounting for the time value of money. Therefore, it allows consistent comparison between options with different costs and output structures (Chen et al., 2021). It is calculated as the ratio of discounted life-cycle costs to discounted electricity generation:

$$LCOE = \frac{\sum_{t=0}^{N} \frac{C_t}{(1+r)^t}}{\sum_{t=1}^{N} \frac{E_t}{(1+r)^t}} \quad (1)$$

where, C_t is the total cost in the year t(USD/m^2), including initial investment (CAPEX at $t = 0$), annual operating costs (OPEX), and any replacement costs. E_t is the AC electricity delivered in year t(kWh/m^2·year). The parameter r is the real discount rate, and N is the system lifetime in years. And the unit is USD/kWh.

The discounted payback period is the time it takes for discounted revenues to recover discounted costs. In other words, it is the first year in which the cumulative discounted net cash flow becomes zero or positive (Chen et al., 2021). It is defined as:

$$\text{Payback} = \min\left\{T : \sum_{t=0}^{T} \frac{R_t - C_t}{(1+r)^t} \geq 0\right\} \quad (2)$$

where, R_t is the revenue in year t(USD/m^2·year), calculated as:

$$R_t = E_t \cdot p$$

where, p is the electricity value (USD/kWh). The unit is years. Discounted return on investment (ROI) measures profitability by comparing discounted net benefits (revenues minus costs) with total discounted costs, expressed as a percentage (Chen et al., 2021). A higher ROI indicates a stronger financial return under the same assumptions:

$$\mathrm{ROI}(\%) = \left(\frac{\sum_{t=0}^{N} \frac{R_t - C_t}{(1+r)^t}}{\sum_{t=0}^{N} \frac{C_t}{(1+r)^t}} \right) \times 100 \quad (3)$$

All variables are defined above, and both costs and revenues are expressed on a per-square-meter façade basis to remain consistent with the study's functional unit. The unit is a percentage.

3.6.3. Economic realism cases (combined assumptions)

To address uncertainty in financing conditions and electricity pricing, the techno-economic analysis is extended by introducing combined "economic realism" cases. Instead of changing one parameter at a time, these cases adjust key inputs together. They are based on the parameter ranges already defined in the sensitivity analysis. The objective is to examine whether the relative feasibility of transparent PV with AI support remains stable under less favorable economic conditions. Three cases are defined and applied across all sites and scenarios in the Results section (see Section 4.3.4).

In the base case (E0), the electricity value is set at $p = 0.07$ USD/kWhand the discount rate at $r = 6\%$. This case aligns with the assumptions used in Table 5 and the main KPI evaluation. In the moderate case (E1), the electricity value decreases to $p = 0.05$ USD/kWh, while the discount rate increases to $r = 8\%$, reflecting lower revenue and moderately higher financing costs. In the stress case (E2), the electricity value remains at $p = 0.05$ USD/kWh, but the discount rate rises further to $r = 10\%$, representing a higher-risk environment with stronger discounting effects.

All other parameters, including capital cost (CAPEX), operating cost rate (OPEX), system lifetime N, degradation, and replacement assumptions are kept at their baseline values unless stated otherwise. Therefore, any differences in results can be directly attributed to the combined economic conditions. The effects of these cases on LCOE, discounted payback period, ROI, and the break-even assessment for AI/controls are presented and discussed in Section 4.3.4, highlighting the conditions under which the advantage of Scenario S3 may decrease or become less attractive.

3.7. CO_2 impact model

3.7.1. Operational avoided CO_2 (existing boundary)

Operational avoided carbon dioxide (CO_2) emissions are estimated by multiplying the electricity generated by the system with a grid emission factor, using a boundary that considers only operational effects. This approach assumes that electricity produced by the PV system replaces grid electricity and therefore reduces emissions associated with conventional generation (Chenic et al., 2022).

For each site and scenario, the avoided CO_2 is calculated as:

$$\mathrm{CO}_{2,\mathrm{avoided}}^{\mathrm{op}} = E_{\mathrm{AC}} \times EF$$

where, E_{AC} represents the annual AC electricity delivered (kWh/m²·year), and $EF$is the grid emission factor (kgCO_2/kWh). The system boundary includes only operational emissions and does not consider embodied emissions from manufacturing, transport, installation, or end-of-life stages, which are typically addressed in full life-cycle assessments (Al-Shetwi, 2022; Chenic et al., 2022). The same emission factor is applied across all sites because grid carbon intensity is treated as a national-level parameter rather than a location-specific value. These assumptions are summarized in Table 6.

Table 6: Emissions assumptions

Item	NEOM	Riyadh	Red Sea project	AlUla
Grid emission factor, EF(kgCO_2/kWh)	0.62	0.62	0.62	0.62
Accounting boundary	Operational only	Operational only	Operational only	Operational only
CO_2 metric reported	kgCO_2 avoided per m² per year	kgCO_2 avoided per m² per year	kgCO_2 avoided per m² per year	kgCO_2 avoided per m² per year

3.7.2. Embodied CO_2 screening (simplified LCA)

To complement the operational-only boundary, a simplified screening of embodied CO_2 is included to capture the potential importance of material and system-related emissions in building-integrated applications. This screening is intended for decision support and does not replace a full life-cycle assessment. It estimates embodied emissions for the main façade and system components and converts them into an annualized value over the project lifetime. The components considered include glass (IGU assembly), framing and integration elements, PV laminate or transparent PV layer, inverter and power electronics, AI/controls hardware, and replacement events such as inverter or control-system updates.

The total embodied CO_2 per square meter is calculated as:

$$\mathrm{CO}_{2,\mathrm{emb,tot}} = \sum_j \left(Q_j \times EF_j^{\mathrm{emb}}\right) + \sum_k \left(Q_k^{\mathrm{rep}} \times EF_k^{\mathrm{emb}}\right) \quad (4)$$

where, Q_j is the quantity of component $j$per m², and $EF_j^{\mathrm{emb}}$is its embodied emission factor (kgCO_2e per unit). The second term accounts for replacement components over the system lifetime. To allow comparison with annual operational savings, the embodied CO_2 is converted into an annual value:

$$CO_{2,\mathrm{emb,ann}} = \frac{CO_{2,\mathrm{emb,tot}}}{N} \quad (5)$$

where, N is the project lifetime in years.

A net CO_2 benefit indicator is then defined as:

$$CO_{2,\mathrm{net}} = CO_{2,\mathrm{avoided}}^{\mathrm{op}} - CO_{2,\mathrm{emb,ann}} \quad (6)$$

A positive value indicates that the emissions avoided during operation exceed the annualized embodied emissions, while a negative value suggests that embodied impacts are greater under the given assumptions. Table 7 outlines the structure of the embodied CO_2 screening inventory, including the main components and the literature-based emission factors used. Because these factors can vary depending on manufacturing processes and data sources, the results are intended to provide approximate guidance and are supported by sensitivity analysis (Section 3.8).

3.8. Sensitivity analysis

A one-factor-at-a-time (OFAT) sensitivity analysis was used to assess how stable the results remained when key inputs were uncertain, particularly those related to harsh-climate losses and financial assumptions. In this approach, one parameter was changed at a time while all others were kept constant, and the resulting variation in outputs was summarized using tornado-style ranges for the key indicators used in decision-making (Chen et al., 2021). Sensitivity testing focused on four decision-relevant outcomes: LCOE (USD/kWh), payback period (years), ROI (%), and operational avoided CO_2 ($kgCO_2/m^2/year$).

The base case relied on the parameter set reported in Table 8, and then selected inputs were adjusted within ranges intended to reflect realistic uncertainty for façade-integrated solar under hot-arid, dust-prone conditions, as well as common uncertainty in project finance inputs used in PV/BIPV assessments (Ang et al., 2022; Chen et al., 2021).

3.9. Statistical analysis

Hourly simulated AC electricity outputs were aggregated to monthly and annual values and analyzed using paired, within-site comparisons to isolate the incremental effect of AI enablement. The primary comparison was the difference between **S3** (AI-enabled transparent PV) and S2 (transparent PV without AI) for each site across the following outputs: annual energy yield ($kWh/m^2/year$), LCOE (USD/kWh), payback period (years), ROI (%), and operational avoided CO_2 ($kgCO_2/m^2/year$). AI impact was reported as an absolute change. $\Delta X = X_{S3} - X_{S2}$ and relative change $\Delta X\% = \frac{X_{S3}-X_{S2}}{X_{S2}} \times 100$, summarized across sites using mean, standard deviation, and min–max ranges. Sensitivity results were summarized as the KPI spread between low and high parameter bounds and ranked by absolute KPI change to support tornado-plot interpretation. Given the small number of sites (n = 4), significance testing was treated as supplementary; when reported, a paired non-parametric Wilcoxon signed-rank test compared S3 versus S2 across sites, and p-values were interpreted cautiously as evidence of directional consistency rather than population-level inference.

4. Results and discussion

4.1. Cross-site KPI overview and comparative summary

4.1.1. Consolidated KPI dashboard (all sites × all scenarios)

Table 9 summarizes the key performance indicators (KPIs) for the four locations across the three scenarios (S1–S3), reported per square meter of façade. Table 9 reports the base-case scenario set (S1–S3); maintenance-constrained AI operation (S3b) results are reported separately in Sections 4.2.4 and 4.3.4 to preserve the comparability of the main KPI dashboard. Across all sites, S1 (Traditional PV) produced the highest annual energy output and showed the strongest economic performance. In comparison, S2 (transparent PV without AI) resulted in a substantial drop in electricity generation and, therefore, less favorable economic outcomes. However, S3 (AI-enabled transparent PV) consistently outperformed S2 across all locations. Annual yield increased by 68.7–77.6 $kWh/m^2/year$ (8.75–9.22%). In addition, LCOE declined by 0.007 USD/kWh (7.37–7.87%), payback time shortened by 1.2–1.3 years (8.05–8.84%), and ROI rose by 0.8–0.9 percentage points (11.76–12.68%). As a result, avoided operational CO_2 also increased by 2.1–2.2 $kgCO_2/m^2/year$ (9.09–9.36%), indicating improved environmental performance compared with S2.

4.1.2. Cross-site statistical summary of AI impact

Table 10 reports the added effect of enabling AI, calculated as the difference between S3 and S2 (S3 − S2), across the four sites for all study KPIs. On average, the AI layer increased the annual energy yield by 73.6 ± 3.7 $kWh/m^2/year$ (range: 68.7 to 77.6), corresponding to a mean relative improvement of 9.02% ± 0.21%. The economic outcomes followed the same pattern across locations.

Specifically, LCOE declined by 0.007 USD/kWh (mean relative change −7.61% ± 0.21%), payback time decreased by 1.23 ± 0.05 years (mean relative change −8.41% ± 0.33%), and ROI rose by 0.88 ± 0.05 percentage points (mean relative change 12.28% ± 0.40%). In addition, operational avoided CO_2 increased by 2.15 ± 0.06 $kgCO_2/m^2/year$, corresponding to a mean relative gain of 9.23% ± 0.11%. All sites showed the same direction of change across all KPIs (4/4), demonstrating strong consistency in the observed impact.

Table 7: Embodied CO_2 screening inventory (components and literature-based factors) (per m^2 façade basis)

Component	Quantity basis (per m^2)	Embodied CO_2 factor (literature-based)	Included items/notes
IGU/glass	kg/m^2 (glass mass)	kgCO_2e/kg glass	Glass panes and spacer; treated as IGU assembly
Frame & façade integration	kg/m^2 (metal mass)	kgCO_2e/kg aluminum (or equivalent)	Frames, brackets, seals, mounting interfaces
PV laminate / TPV layer	per m^2 module area	kgCO_2e/m^2 module (or per W)	Transparent PV layer within module
Inverter & power electronics	allocated per m^2	kgCO_2e per share	Includes replacement at Year 13
AI/controls hardware	allocated per m^2	kgCO_2e per share	Sensors, gateway, communication devices; refresh at Year 10 if applicable
Replacement events	event-based	matched to component	Includes inverter and control-system replacements

This screening extends the environmental assessment beyond operational emissions by estimating annualized embodied CO_2. It is intended as a simplified approach rather than a full life-cycle assessment and is used to calculate a net CO_2 benefit indicator for comparison purposes

Table 8: Sensitivity inputs and ranges

Parameter	Symbol	Unit	Low	Base	High
Total CAPEX (per m^2)	CAPEX	USD/m^2	−25%	1.00×	+25%
Annual OPEX rate	OPEX	% of CAPEX/yr	1.5%	2.0%	3.0%
Discount rate	r	%	4.0	6.0	10.0
Project lifetime	N	years	20	25	30
Annual degradation rate (TPV)	d	%/yr	0.4	0.8	1.2
Average soiling loss (TPV, non-AI)	L_{soil}	%	4	8	12
AI/controls premium (scenario 3)	C_{AI}	USD/m^2	20	35	60
AI effect on soiling (scenario 3 effective loss)	$L_{soil,S3}$	%	4.5	6.0	7.5
Electricity value	p	USD/kWh	0.05	0.07	0.10
Grid emission factor	EF	kgCO_2/kWh	0.45	0.62	0.80

Table 9: Key performance indicators by location and scenario (per m^2 façade basis), including uplift from S3 relative to S2

Panel A: Energy and CO_2 KPIs (per m^2 façade basis)

Location	Yield S1 (kWh/m^2/yr)	Yield S2	Yield S3	AI uplift (Δ, %)	CO_2 S1 (kg/m^2/yr)	CO_2 S2	CO_2 S3	AI uplift (Δ, %)
AlUla	1904.2	841.5	919.1	+77.6 (9.22%)	53.4	23.8	26.0	+2.2 (9.24%)
NEOM	1860.4	820.7	894.5	+73.8 (8.99%)	52.3	23.5	25.7	+2.2 (9.36%)
Red Sea	1821.7	812.3	886.4	+74.1 (9.12%)	51.6	23.1	25.2	+2.1 (9.09%)
Riyadh	1795.1	785.4	854.1	+68.7 (8.75%)	50.8	22.8	24.9	+2.1 (9.21%)

Panel B: Techno-economic KPIs (per m^2 façade basis)

Location	**LCOE S1 (USD/kWh)**	**LCOE S2**	**LCOE S3**	**AI uplift (Δ, %)**	**Payback S1 (yr)**	**Payback S2**	**Payback S3**	**AI uplift (Δ, %)**	**ROI S1 (%)**	**ROI S2**	**ROI S3**	**AI uplift (Δ, %)**
AlUla	0.043	0.089	0.082	−0.007 (−7.87%)	6.8	14.2	13.0	−1.2 (−8.45%)	15.0	7.4	8.3	+0.9 (12.16%)
NEOM	0.045	0.091	0.084	−0.007 (−7.69%)	7.2	14.5	13.3	−1.2 (−8.28%)	14.6	7.2	8.1	+0.9 (12.50%)
Red Sea	0.046	0.093	0.086	−0.007 (−7.53%)	7.6	14.7	13.4	−1.3 (−8.84%)	14.3	7.1	8.0	+0.9 (12.68%)
Riyadh	0.048	0.095	0.088	−0.007 (−7.37%)	7.9	14.9	13.7	−1.2 (−8.05%)	13.9	6.8	7.6	+0.8 (11.76%)

Δ and %Δ were computed as S3 − S2 and (S3 − S2)/S2 × 100, respectively

4.2. Energy performance of transparent BIPV façades

4.2.1. Annual energy yield by scenario and site

Fig. 2 compares the annual energy yield per unit façade area for the three scenarios (S1–S3) across NEOM, Riyadh, the Red Sea site, and AlUla. Across all locations, the traditional PV option (S1) delivered the greatest yearly output, ranging from 1795.1 to 1904.2 kWh/m^2/year. This higher yield is mainly due to the stronger conversion performance of non-transparent (opaque) modules when they receive the same solar input. In contrast, the transparent PV case without enhanced control (S2) produced much less energy, ranging from 785.4 to 841.5 kWh/m^2/year. As a result, S2 showed an output reduction of about 55.4%–56.2% compared with S1, indicating that improved visibility through the façade comes at a significant energy cost.

When enhanced operational control was introduced (S3), the annual yield increased to 854.1–919.1 kWh/m^2/year. Therefore, this improvement narrowed the performance gap linked to transparency, but did not eliminate it. Even with these operational gains, S3 remained about 51.3%–52.4% below S1.

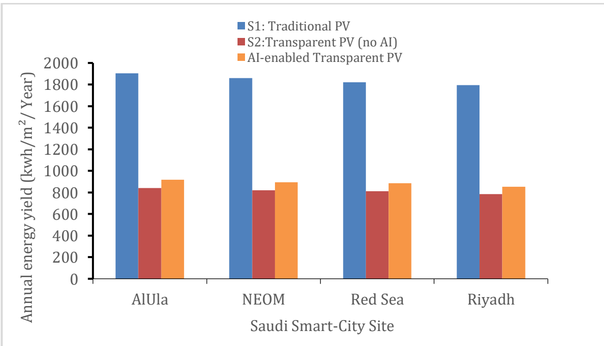

Fig. 2: Annual energy yield by scenario across sites

Overall, the findings suggest that better operation can recover part of the energy lost in transparent façade designs; however, the basic balance between letting light through and producing electricity continues to limit the total yield.

Table 10: Cross-site statistical summary of AI effect (S3 vs. S2) for all KPIs

KPI	Δ(S3−S2) mean	SD	Min	Max	%Δ (S3 vs. S2) mean	SD	Min	Max
Annual energy yield (kWh/m²/year)	73.6	3.7	68.7	77.6	9.02	0.21	8.75	9.22
LCOE (USD/kWh)	−0.0070	0.0000	−0.0070	−0.0070	−7.61	0.21	−7.87	−7.37
Payback period (years)	−1.23	0.05	−1.30	−1.20	−8.41	0.33	−8.84	−8.05
ROI (percentage points)	0.88	0.05	0.80	0.90	12.28	0.40	11.76	12.68
Avoided CO_2 ($kgCO_2/m^2$/year)	2.15	0.06	2.10	2.20	9.23	0.11	9.09	9.36

4.2.2. Incremental energy gains attributable to AI enablement (S3 vs. S2)

Table 11 summarizes the added annual energy produced when the AI-enabled transparent façade scenario (S3) is compared with the transparent baseline (S2) across the four Saudi smart-city sites. It reports the annual façade-normalized yields for S2 and S3, along with the absolute gain (Δ) and the percentage increase for each location. Overall, Table 11 shows a consistent improvement in output with S3, with absolute gains ranging from 68.7 to 77.6 kWh/m²/year and relative increases of 8.75% to 9.22% across NEOM, Riyadh, the Red Sea site, and AlUla.

Table 11: AI contribution to annual energy yield by site (S3 vs. S2)

Site	S2 (kWh/m²/year)	S3 (kWh/m²/year)	Δ (S3–S2) (kWh/m²/year)	%Δ (S3 vs. S2)
NEOM	820.7	894.5	73.8	8.99%
Riyadh	785.4	854.1	68.7	8.75%
Red Sea	812.3	886.4	74.1	9.12%
AlUla	841.5	919.1	77.6	9.22%

Fig. 3 separates the added energy benefit of the S3 approach by directly comparing it with the transparent reference case (S2). Across NEOM, Riyadh, the Red Sea site, and AlUla, S3 increased the façade-normalized annual yield by 68.7 to 77.6 kWh/m²/year. In relative terms, this corresponds to an improvement of 8.75% to 9.22%, depending on the site. In addition, the differences in uplift between locations were small, which indicates that the S3 operating approach provided a broadly consistent advantage across the range of Saudi climate conditions considered.

However, the small variations observed across sites can reasonably be linked to local conditions that influence both available sunlight and system losses. For example, differences in temperature-related performance reduction, dust and soiling buildup, and the angle at which sunlight strikes the façade can all affect how much extra energy is recovered at each location. As a result, even with the same operating approach, the uplift is expected to shift slightly from one site to another.

From an operational perspective, the S3 approach mainly functioned as a yield-recovery measure for transparent façades. It improved the output of the transparent system compared with S2; nevertheless, it did not change the overall standing of transparent PV relative to conventional PV, since traditional modules still produced substantially more energy in absolute terms.

4.2.3. Monthly and seasonal behavior (mechanistic interpretation)

Fig. 4 shows the month-by-month energy-yield patterns for the transparent façade scenarios (S2 and S3). Across all sites, production generally increased from late winter into spring and then declined during the summer-to-winter transition. This seasonal behavior aligns with the combined effects of solar-angle changes throughout the year, shifts in outdoor temperatures, and dust and surface-soiling losses. In addition, the S3 line remains above S2 in every month, indicating that the improvement is steady over time rather than confined to a single season.

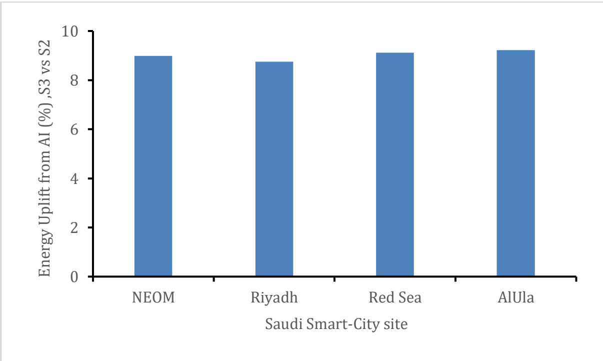

Fig. 3: AI energy uplift (%Δ S3 vs. S2) by site

From an operational standpoint, the largest month-to-month gaps between S3 and S2 occurred when the baseline output was already high. Therefore, when conditions supported stronger generation, better operation, and loss control translated into a larger amount of energy recovered per square meter. As a result, the monthly profiles support the view that S3 improves yield mainly through ongoing reductions in cumulative losses and more effective operating decisions throughout the year.

4.2.4. Maintenance-constrained AI operation (S3b)

To reflect practical façade-access limitations for high-rise buildings, Scenario S3b (maintenance-constrained AI-enabled transparent PV) is evaluated as a conservative feasibility case in which the same transparent PV configuration and AI decision logic as S3 are retained, but cleaning execution is constrained by access scheduling and delayed work-order implementation at height. In simulation terms, this constraint reduces the realized loss-recovery benefit relative to S3 because condition-based cleaning triggers cannot always be executed at the optimal time. Consequently, the annual yield uplift in S3b is lower than in S3 and represents a practical lower-bound estimate of the achievable operational gain under constrained façade maintenance. Table 12 summarizes the resulting annual yields and quantifies the reduced uplift relative to S2, alongside the shortfall relative to the unconstrained S3 case.

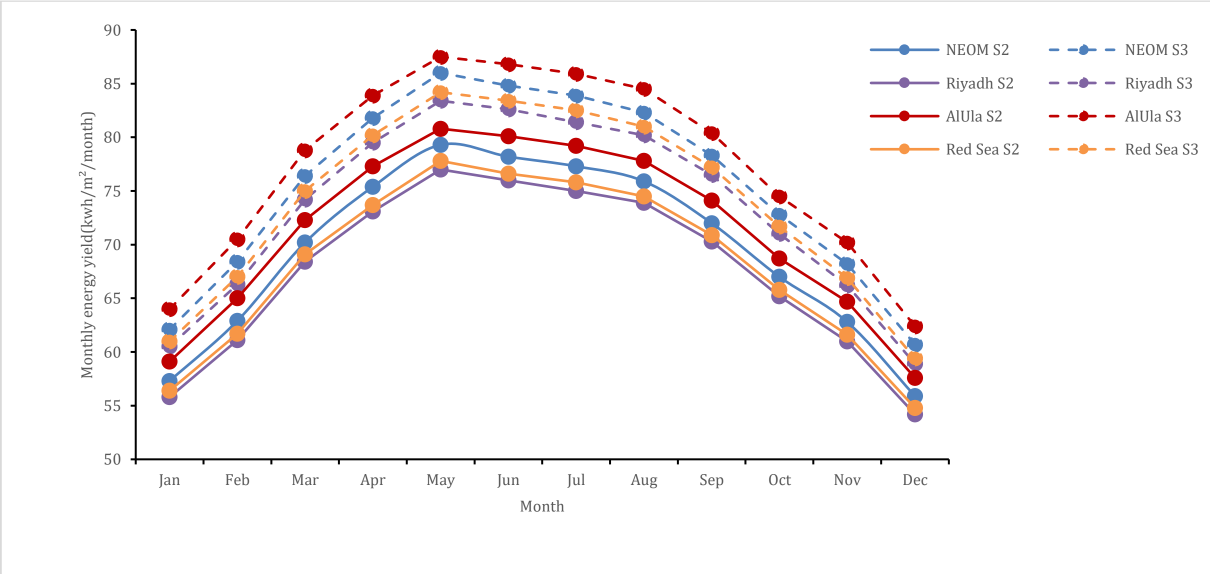

Fig. 4: Monthly energy yield profiles (S2 vs. S3) for each site

Table 12: Maintenance-constrained AI contribution to annual energy yield by site (S3b vs. S2 and S3)

Site	S2 yield (kWh/m²·yr)	S3 yield (kWh/m²·yr)	S3b yield (kWh/m²·yr)	Δ(S3b–S2) (kWh/m²·yr)	%Δ (S3b vs. S2)	Δ(S3–S3b) (kWh/m²·yr)
NEOM	820.7	894.5	857.6	36.9	4.50%	36.9
Riyadh	785.4	854.1	819.8	34.4	4.37%	34.4
Red Sea	812.3	886.4	849.4	37.1	4.56%	37.1
AlUla	841.5	919.1	880.3	38.8	4.61%	38.8

Δ(S3b–S2) is computed as S3b − S2, and %Δ (S3b vs. S2) is computed as (S3b − S2)/S2 × 100. Δ(S3–S3b) is computed as S3 − S3b. By construction, S3b falls between S2 and S3, indicating partial realization of AI-enabled loss recovery under maintenance constraints. The implications of this reduced yield recovery on LCOE, payback, and ROI are reported in Section 4.3.4 (maintenance-constrained economics)

4.3. Techno-economic outcomes

4.3.1. Levelized cost of electricity (LCOE) across scenarios and sites

Table 13 summarizes the levelized cost of electricity (LCOE) for each site under scenarios S1–S3. It also reports the absolute and percentage change when moving from the transparent baseline (S2) to the improved transparent case (S3), which helps quantify the cost impact of the added operational improvement.

Table 13: LCOE by location and scenario (per m² façade basis)

Site	LCOE S1 (USD/kWh)	LCOE S2	LCOE S3	Δ(S3–S2)	%Δ (S3 vs. S2)
AlUla	0.043	0.089	0.082	−0.007	−7.87%
NEOM	0.045	0.091	0.084	−0.007	−7.69%
Red Sea	0.046	0.093	0.086	−0.007	−7.53%
Riyadh	0.048	0.095	0.088	−0.007	−7.37%

Fig. 5 presents the same LCOE results visually, making it easier to compare scenario performance across locations at a glance and to see the consistent cost reduction from S2 to S3.

Across all sites, S1 delivered the lowest LCOE (0.043–0.048 USD/kWh), mainly because its higher annual energy output spreads costs over more generated electricity. In contrast, S2 recorded the highest LCOE (0.089–0.095 USD/kWh) because the transparent façade produced less energy per m² while still requiring similar supporting components. However, S3 reduced LCOE to 0.082–0.088 USD/kWh, representing a consistent improvement of −0.007 USD/kWh (−7.37% to −7.87%) compared with S2.

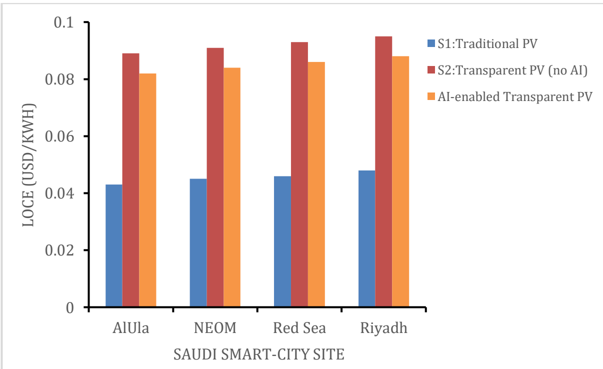

Fig. 5: LCOE by scenario and site

The LCOE reduction in S3 was mainly driven by increased annual energy production, which improved the energy term used in the LCOE calculation. Therefore, even though S3 included an added cost component, that increase was small relative to the extra electricity produced. As a result, relatively small yearly gains can still lead to clear LCOE improvements when the project lifetime and discount assumptions remain fixed (Chen et al., 2021).

4.3.2. Payback period and ROI: Investment attractiveness

Table 14 compiles the payback period and return on investment (ROI) for each site under scenarios S1–S3. In addition to listing the site-specific values, Table 14 reports the absolute and percentage changes from the transparent baseline (S2) to the improved transparent case (S3), helping clarify the extent to which the added operational improvement affects financial performance. Fig. 6 and Fig. 7 present the same results in chart form, making it easier to compare sites and scenarios at a glance. Fig. 6 highlights differences in payback time, while Fig. 7 shows how ROI shifts across locations for each scenario.

Table 14: Payback and ROI by location and scenario (per m² façade basis)

Site	Payback S1 (yr)	Payback S2	Payback S3	Δ(S3–S2) (yr)	%Δ	ROI S1 (%)	ROI S2	ROI S3	Δ(S3–S2) (pp)	%Δ
AlUla	6.8	14.2	13.0	−1.2	−8.45%	15.0	7.4	8.3	+0.9	+12.16%
NEOM	7.2	14.5	13.3	−1.2	−8.28%	14.6	7.2	8.1	+0.9	+12.50%
Red Sea	7.6	14.7	13.4	−1.3	−8.84%	14.3	7.1	8.0	+0.9	+12.68%
Riyadh	7.9	14.9	13.7	−1.2	−8.05%	13.9	6.8	7.6	+0.8	+11.76%

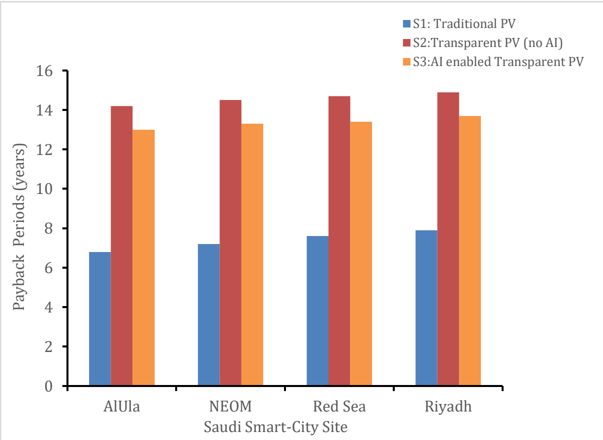

Fig. 6: Payback period by scenario and site

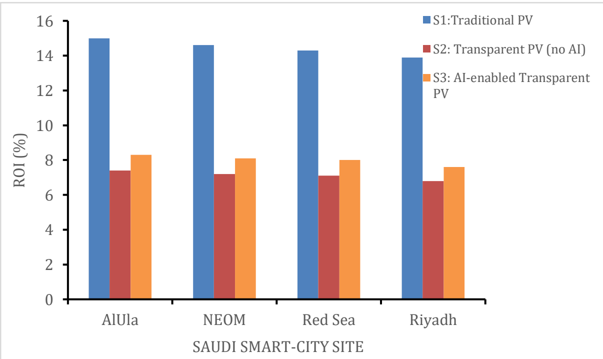

Fig. 7: ROI by scenario and site

Across all sites, S1 had the strongest investment profile, with the shortest payback period (6.8–7.9 years) and the highest ROI (13.9%–15.0%). In contrast, S2 showed the weakest performance, with payback times of 14.2–14.9 years and an ROI of 6.8%–7.4%. This pattern reflects the reduced electricity output of the transparent façade configuration, which slows cost recovery and limits returns under otherwise comparable project assumptions.

S3 improved both indicators relative to S2. Payback decreased to 13.0–13.7 years, which equals a reduction of about 1.2–1.3 years (−8.05% to −8.84%), while ROI increased to 7.6%–8.3%, representing an improvement of +0.8 to +0.9 percentage points (+11.76% to +12.68%). The largest absolute ROI gains were observed at AlUla and NEOM, aligning with their higher annual energy production and slightly larger output recovery. Overall, the financial improvements followed the energy gains more closely than the minor cost differences between sites.

4.3.3. Economic interpretation for façade deployment decisions

The techno-economic findings point to a clear trade-off among the scenarios. The transparent façade option (S2) supports daylighting and architectural integration; however, it delivers noticeably lower annual electricity output and weaker financial results than the traditional PV case (S1). By comparison, the enhanced transparent façade option (S3) partly improves this balance by recovering some of the lost generation through better operation and reduced losses. As a result, S3 shows stronger cost performance (lower LCOE) and more attractive investment indicators (shorter payback and higher ROI) than S2, even though the transparency-related limit on total output remains in place.

To support practical façade deployment decisions, a simple screening check compares the added upfront premium for the S3 operating layer with the discounted value of the extra electricity generated relative to S2. Table 15 summarizes this comparison using a constant electricity value, a fixed discount rate, and a defined project lifetime. Under these assumptions, the present value of the recovered electricity ranges from about 59 to 67 USD/m², which is higher than the assumed premium of 35 USD/m² for every site. Therefore, the added feature remains financially reasonable as long as its cost stays below the monetized value of the energy it helps recover.

Fig. 8 provides a visual version of this break-even screen by placing the present value of the added electricity next to the assumed premium for each site. This presentation clearly shows that the value of the recovered output remains above the upfront cost in all cases.

Table 15: AI premium break-even screen (per m^2 façade basis)

Site	ΔE ($kWh/m^2/yr$)	Annual value ($USD/m^2/yr$)	Present value of uplift (USD/m^2)	Assumed AI premium (USD/m^2)	Present value uplift/premium	Simple premium payback (yr)
AlUla	77.6	5.43	67.3	35.0	1.92	6.44
NEOM	73.8	5.17	64.0	35.0	1.83	6.77
Red Sea	74.1	5.19	64.2	35.0	1.83	6.75
Riyadh	68.7	4.81	59.5	35.0	1.70	7.28

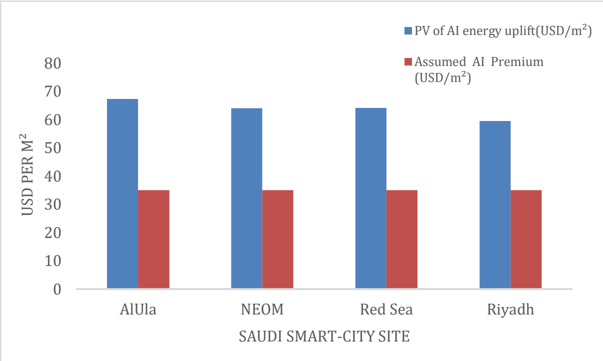

Fig. 8: Present value of uplift versus assumed AI premium

4.3.4. Maintenance-constrained economics (S3b) and implications for feasibility

Scenario S3b, which represents maintenance-constrained AI-enabled transparent PV, uses the same transparent façade design and AI/controls cost assumptions as S3. However, it assumes that limited façade access delays or restricts condition-based cleaning. As a result, the amount of energy recovered is lower than in S3 (Section 4.2.4). This reduction directly limits the economic benefits that were achieved in S3 through higher electricity output. Table 16 presents the LCOE, discounted payback period, and ROI for S3b. In general, S3b still performs better than S2, which represents transparent PV without AI, but it is less effective than S3 at all sites. Under S3b, LCOE rises to 0.085–0.092 USD/kWh, payback increases to 13.6–14.3 years, and ROI falls to 7.2%–7.9%. These results show that maintenance constraints allow only partial recovery of operational losses rather than the fuller recovery achieved in S3.

Table 16: Maintenance-constrained techno-economic KPIs by site (S3b vs. S2 and S3; per m^2 façade basis)

Site	LCOE S2 (USD/kWh)	LCOE S3	LCOE S3b	Payback S2 (yr)	Payback S3	Payback S3b (yr)	ROI S2 (%)	ROI S3 (%)	ROI S3b (%)
AlUla	0.089	0.082	0.086	14.2	13.0	13.6	7.4	8.3	7.9
NEOM	0.091	0.084	0.088	14.5	13.3	13.9	7.2	8.1	7.7
Red Sea	0.093	0.086	0.090	14.7	13.4	14.1	7.1	8.0	7.6
Riyadh	0.095	0.088	0.092	14.9	13.7	14.3	6.8	7.6	7.2

S3b follows the same investment and O&M assumptions as S3, but it produces less delivered electricity because maintenance actions are more difficult to implement. Therefore, its LCOE is higher and its payback period is longer than in S3. The S3b results remain between S2 and S3, consistent with the idea that AI-enabled monitoring reduces some operational losses, but maintenance work cannot always be completed at the optimal time

The maintenance limitation also changes the break-even assessment in Table 15. Since S3b provides a smaller energy gain than S3, the present value of the recovered electricity also decreases. As a result, the difference between the present value of the electricity uplift and the AI premium becomes narrower. In the S3b case, the present value of recovered electricity ranges from 29.8 to 33.6 USD/m^2, depending on the site. This is below the assumed AI/controls premium of 35 USD/m^2, giving present value-uplift-to-premium ratios of around 0.85–0.96. Therefore, when maintenance is constrained, particularly at the lower-performing site, Riyadh, the added AI/controls layer may not be financially justified under the base-case electricity value and discounting assumptions. However, it may become feasible if the AI/controls premium decreases through scale or better integration, if electricity value increases through higher tariffs or stronger on-site kWh value, or if access improves through robotic or drone cleaning and planned façade-maintenance systems that allow performance closer to S3.

4.3.5. Economic realism cases (combined discount rate and electricity value assumptions)

To examine whether the S3 advantage remains strong under less favorable economic conditions, the techno-economic KPIs were recalculated using the combined "economic realism" cases described in Section 3.6.3. These cases, E0 to E2, vary the electricity value $p$and discount rate r together to represent more conservative tariff and financing assumptions than the base case. Table 17 presents the resulting LCOE, discounted payback period, and ROI for the transparent façade scenarios (S2 and S3) across all sites.

Across all sites, S3 continues to perform better than S2 under the combined realism cases, with lower LCOE, shorter payback, and higher ROI. However, the overall financial attractiveness decreases as the electricity value falls and the discount rate rises. Under E1, payback increases to about 18.7–21.5 years, while ROI declines to around 4.6%–5.6%. Under E2, payback increases further to 19.3–22.1 years, and ROI falls to 4.4–5.4%. Therefore, although S3 remains the stronger option in relative terms, façade PV may become less attractive for projects that require shorter payback periods.

The break-even interpretation also becomes stricter under E2. Since the present value of recovered electricity depends on both p and r. The financial value of the S3 improvement over S2 may fall below the AI/controls premium of about 35 USD/m^2, especially at the weaker-performing site, Riyadh. As a result, S3 adoption under conservative tariff and financing conditions depends on lowering AI/controls costs, improving realized energy recovery through feasible maintenance, or increasing the value assigned to façade-generated electricity.

Table 17: Economic realism cases (combined assumptions): Techno-economic KPIs for S2 vs. S3 (per m^2 façade basis)

Site	Case	p(USD/kWh)	r	LCOE S2	LCOE S3	Payback S2	Payback S3	ROI S2	ROI S3
AlUla	E0 (Base)	0.07	6%	0.089	0.082	14.2	13.0	7.4	8.3
AlUla	E1 (Moderate)	0.05	8%	0.102	0.094	20.5	18.7	5.0	5.6
AlUla	E2 (Stress)	0.05	10%	0.116	0.107	21.1	19.3	4.8	5.4
NEOM	E0 (Base)	0.07	6%	0.091	0.084	14.5	13.3	7.2	8.1
NEOM	E1 (Moderate)	0.05	8%	0.104	0.096	20.9	19.2	4.9	5.5
NEOM	E2 (Stress)	0.05	10%	0.118	0.109	21.5	19.7	4.7	5.3
Red Sea	E0 (Base)	0.07	6%	0.093	0.086	14.7	13.4	7.1	8.0
Red Sea	E1 (Moderate)	0.05	8%	0.107	0.099	21.2	19.3	4.8	5.4
Red Sea	E2 (Stress)	0.05	10%	0.121	0.112	21.8	19.9	4.6	5.2
Riyadh	E0 (Base)	0.07	6%	0.095	0.088	14.9	13.7	6.8	7.6
Riyadh	E1 (Moderate)	0.05	8%	0.109	0.101	21.5	19.8	4.6	5.2
Riyadh	E2 (Stress)	0.05	10%	0.124	0.114	22.1	20.3	4.4	4.9

LCOE is mainly affected by the discount rate r, while both electricity value influences discounted payback and ROI $p$and discount rate r. The base case E0 follows the main KPI assumptions, while E1 and E2 apply the more conservative combined assumptions defined in Section 3.6.3

4.4. Operational CO_2 avoidance outcomes

4.4.1. Annual avoided CO_2 by scenario and site (operational boundary)

Avoided operational CO_2 was calculated per unit façade area ($kgCO_2/m^2$/year) using an electricity-displacement boundary only. Under this approach, avoided emissions increase in direct proportion to the electricity delivered, assuming a constant grid carbon-intensity value. Therefore, the indicator remains comparable across sites and scenarios, and differences in avoided CO_2 mainly reflect differences in net annual energy yield rather than changes in the emissions factor.

Table 18 summarizes the avoided CO_2 results by site and scenario. Overall, the conventional PV case (S1) produced the largest avoided emissions at every location, ranging from 50.8 to 53.4 $kgCO_2/m^2$/year. In contrast, the transparent façade baseline (S2) recorded the lowest values (22.8–23.8 $kgCO_2/m^2$/year). The improved transparent façade case (S3) avoided more CO_2 than S2, reaching 24.9–26.0 $kgCO_2/m^2$/year.

As a result, the additional decarbonization benefit of S3 compared with S2 was about +2.1 to +2.2 $kgCO_2/m^2$/year, equal to a +9.09% to +9.36% increase, which closely follows the pattern observed in energy-yield gains.

Table 18: Avoided CO_2 by location and scenario (operational-only; per m^2 façade basis)

Site	S1 ($kgCO_2/m^2$/yr)	S2 ($kgCO_2/m^2$/yr)	S3 ($kgCO_2/m^2$/yr)	Δ(S3–S2) ($kgCO_2/m^2$/yr)	%Δ (S3 vs. S2)
AlUla	53.4	23.8	26.0	+2.2	9.24%
NEOM	52.3	23.5	25.7	+2.2	9.36%
Red Sea	51.6	23.1	25.2	+2.1	9.09%
Riyadh	50.8	22.8	24.9	+2.1	9.21%

Fig. 9 presents the same avoided CO_2 values in bar form, making the ranking across scenarios clearer and highlighting the consistent improvement from S2 to S3 across all sites.

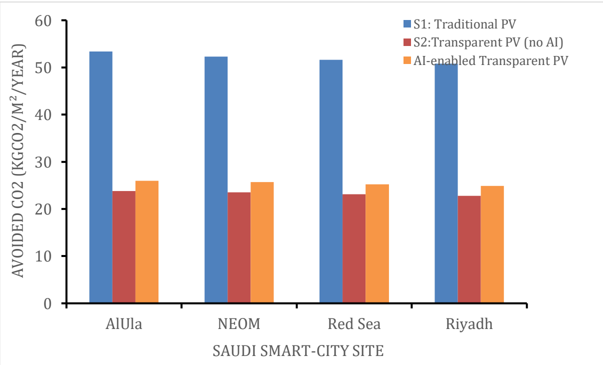

Fig. 9: Avoided CO_2 by scenario and site

Avoided operational carbon dioxide (CO_2) emissions are calculated by multiplying the amount of delivered electricity by a fixed grid emission factor, meaning the results follow a direct linear relationship with annual energy production. Therefore, when electricity output changes, avoided CO_2 changes in the same proportion. Under the maintenance-constrained scenario (S3b), electricity generation is lower than in the unconstrained AI-enabled case (S3). As a result, the avoided CO_2 is also reduced. Table 19 presents the avoided CO_2 values for S3b across different sites, showing that these results fall between S2 and S3. This pattern reflects the partial recovery of energy losses when maintenance actions cannot always be carried out effectively.

Table 19: Operational avoided CO_2 under maintenance-constrained AI operation (S3b) (operational-only; per m^2 façade basis)

Site	CO_2 S2 ($kgCO_2/m^2$·yr)	CO_2 S3 ($kgCO_2/m^2$·yr)	CO_2 S3b ($kgCO_2/m^2$·yr)
AlUla	23.8	26.0	24.9
NEOM	23.5	25.7	24.6
Red Sea	23.1	25.2	24.2
Riyadh	22.8	24.9	23.8

4.4.2. Practical interpretation for façade-scale deployment

For façade-scale planning, reporting avoided CO_2 in $kgCO_2/m^2$/year provides a straightforward scaling rule. Within the operational boundary used in this study, total annual avoided emissions increase roughly in proportion to the installed area of the transparent façade, because avoided CO_2 is directly tied to the amount of electricity delivered under a constant grid carbon-intensity assumption.

Table 20 converts the per-m^2 results into a more practical format by expressing avoided CO_2 per 1,000 m^2 of façade area. Using this scaling, S3 achieves about 24.9–26.0 tCO_2/year per 1,000 m^2, while S2 reaches about 22.8–23.8 tCO_2/year per 1,000 m^2. As a result, the incremental benefit of moving from S2 to S3 is approximately 2.1–2.2 tCO_2/year per 1,000 m^2, with a similar percentage increase across sites.

Table 20: Avoided CO_2 scaled to 1,000 m^2 façade area (tCO_2/year)

Site	S2 (tCO_2/yr per 1,000 m^2)	S3 (tCO_2/yr per 1,000 m^2)	Uplift (tCO_2/yr)	%Δ (S3 vs. S2)
AlUla	23.8	26.0	2.2	9.24%
NEOM	23.5	25.7	2.2	9.36%
Red Sea	23.1	25.2	2.1	9.09%
Riyadh	22.8	24.9	2.1	9.21%

Fig. 10 shows the same comparison, highlighting the additional CO_2 avoided in S3 relative to S2 per 1,000 m^2 of façade. This visual makes it easier to see that the added benefit remains consistent across the four sites.

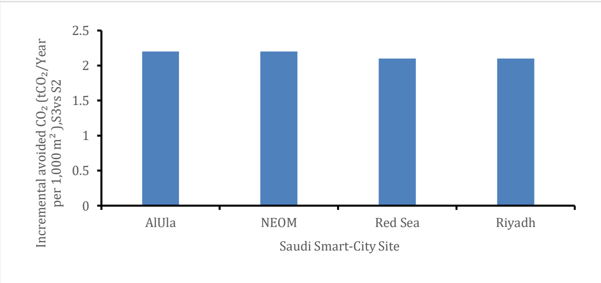

Fig. 10: Incremental avoided CO_2 (S3 vs. S2) per 1,000 m^2 façade

This interpretation remains limited to operational emissions and therefore depends on the selected grid carbon-intensity factor. If the grid's carbon intensity changes, the absolute avoided CO_2 values would rise or fall accordingly; however, the relative improvement from S2 to S3 would still be driven mainly by the difference in annual electricity output between the two scenarios.

4.4.3. Embodied CO_2 screening and net CO_2 benefit

Since building-integrated systems can involve notable embodied emissions from components such as glazing, framing, PV layers, and electronic equipment, an embodied CO_2 screening (Section 3.7.2) is included to complement the operational-only avoided CO_2 results. This screening provides an approximate estimate of embodied emissions for key façade elements, including IGU/glass units, structural framing and integration parts, PV laminate layers, inverter and electronic components, as well as AI-related hardware and associated replacements. These emissions are then converted into an annual value over the assumed project lifetime of $N =$ 25years. Based on this, a net CO_2 benefit is calculated as:

$$CO_{2,\text{net}} = CO_{2,\text{avoided}}^{\text{op}} - CO_{2,\text{emb,ann}}$$

For this analysis, the annualized embodied emissions are treated as scenario-dependent but consistent across sites. Specifically, values of $CO_{2,\text{emb,ann}} = 6.4\text{kg}CO_2\text{e}/\text{m}^2\cdot\text{yr}$ are used for Scenario S2, while $CO_{2,\text{emb,ann}} = 6.6\text{kg}CO_2\text{e}/\text{m}^2\cdot\text{yr}$ are applied to Scenarios S3 and S3b, reflecting the additional contribution from AI and control components, including periodic updates. Table 21 presents the resulting net CO_2 benefits for each site and scenario. The results show that net CO_2 benefits remain positive in all cases under the screening assumptions. Moreover, the ranking follows the level of electricity production, with Scenario S3 achieving the highest net benefit among transparent façade options, while Scenario S3b provides a more conservative estimate due to maintenance limitations.

Table 21: Net CO_2 benefit (operational avoided – annualized embodied) for transparent façade cases ($kgCO_2/m^2\cdot yr$)

Site	Operational avoided CO_2 S2	Net CO_2 S2	Operational avoided CO_2 S3	Net CO_2 S3	Operational avoided CO_2 S3b	Net CO_2 S3b
AlUla	23.8	17.4	26.0	19.4	24.9	18.3
NEOM	23.5	17.1	25.7	19.1	24.6	18.0
Red Sea	23.1	16.7	25.2	18.6	24.2	17.6
Riyadh	22.8	16.4	24.9	18.3	23.8	17.2

Net CO_2 values are calculated using $CO_{2,\text{net}} = CO_{2,\text{avoided}}^{\text{op}} - CO_{2,\text{emb,ann}}$. The annualized embodied emissions applied in this screening are 6.4 $kgCO_2e/m^2\cdot yr$ for S2 and 6.6 $kgCO_2e/m^2\cdot yr$ for S3 and S3b over a 25-year lifetime. These values are intended as approximate estimates for decision support rather than a full life-cycle assessment, and the results may vary depending on assumptions related to material inputs and replacement cycles

4.5. Sensitivity and robustness assessment (OFAT + tornado analysis)

4.5.1. Sensitivity results for techno-economic indicators

A one-factor-at-a-time (OFAT) sensitivity test was conducted to identify which inputs most strongly influence the levelized cost of electricity (LCOE) and payback period for Scenario 3. In this approach, each parameter was adjusted individually, while all other assumptions remained constant. Fig. 11 summarizes the results using a tornado chart, where wider bars indicate a larger effect on LCOE relative to the base case. Fig. 11 shows that the combined cost of transparent PV and façade integration (CAPEX) created the largest change in LCOE, ranging from −6.2% to +6.4%. The next most influential factor was the severity of dust and soiling losses, which shifted LCOE from −5.0% to +5.2%. The added premium for the operating layer (software, sensors, computing, and operations) also had a notable impact, with an LCOE range of −4.0% to +4.2%. In comparison, heat-related performance reduction produced a smaller but still meaningful swing (−3.4% to +3.6%), and the discount rate had a similar secondary influence (−3.0% to +3.1%). Routine operation and maintenance (O&M) costs showed the smallest response among the listed drivers, with a change in LCOE of about −2.6% to +2.8%.

Payback period sensitivity followed a similar pattern. Therefore, installed cost and loss factors that directly affect delivered electricity—especially upfront CAPEX and soiling severity—were the main determinants of investment appeal for Scenario 3. As a result, improving cost control and reducing operational losses would have the greatest leverage in strengthening the financial case for transparent façade deployment under the tested assumptions.

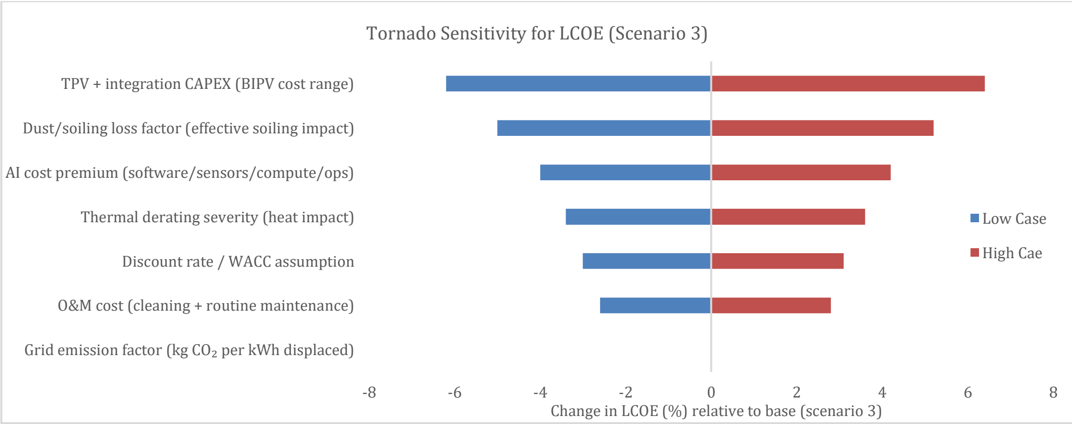

Fig. 11: Tornado plot for LCOE sensitivity (scenario 3)

4.5.2. Sensitivity results for energy and CO_2 outcomes

Sensitivity testing showed that annual energy output was influenced more by environmental loss processes than by cost-related assumptions. The greatest changes in façade-normalized energy yield were linked to dust and soiling conditions, where adjusting soiling-loss severity produced a response of about ±6.0%. Heat-related performance reduction was the next most influential factor, shifting energy yield by roughly ±4.0%. Therefore, the results confirm that harsh-climate operating conditions remain the main drivers shaping annual electricity production for the transparent façade system.

Operational avoided CO_2 followed a different pattern. Because avoided emissions were calculated using a constant grid carbon intensity assumption in each case, changing the grid emission factor produced the largest swing in avoided CO_2, ranging from −20% to +20%. In contrast, soiling and heat-related effects produced smaller secondary changes (approximately ±6% and ±4%, respectively), as they influenced avoided CO_2 indirectly by altering delivered electricity rather than the emissions factor itself. Fig. 12 illustrates this dominance clearly by showing the grid emission factor as the most influential parameter in the avoided CO_2 results.

Across all tested ranges, as illustrated in Fig. 12, the enhanced transparent façade case (S3) maintained a consistent energy advantage over the transparent baseline (S2). As a result, the direction of the S3 benefit remained stable, even though the magnitude of the improvement varied with the severity of losses and the assumptions applied.

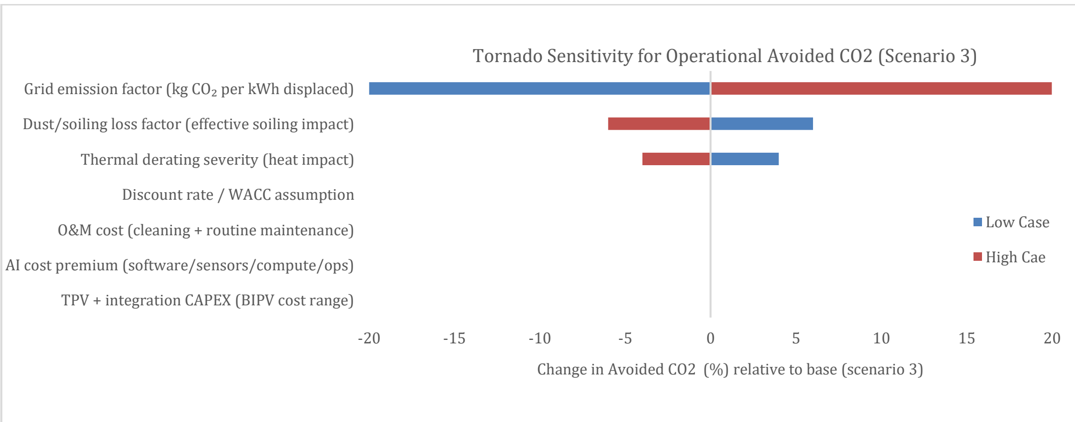

Fig. 12: Tornado plot for avoided CO_2 sensitivity (scenario 3)

4.5.3. Probabilistic uncertainty results (Monte Carlo)

To complement the one-factor-at-a-time (OFAT) sensitivity analysis, a Monte Carlo uncertainty analysis was conducted to provide a probabilistic interpretation of the results. This approach uses the same parameter ranges defined in Table 8 but evaluates them simultaneously to reflect realistic combined uncertainty. In each simulation, key input variables were randomly sampled, and the corresponding KPIs were recalculated to assess how often the AI-enabled scenario (S3) outperforms the transparent baseline (S2). A total of 50,000 simulations were conducted for each site.

The uncertain inputs were modeled using triangular distributions centered on base-case values, unless otherwise specified. Electricity value was sampled as $p \sim \mathrm{Tri}(0.05, 0.07, 0.10)$, and the discount rate as $r \sim \mathrm{Tri}(0.04, 0.06, 0.10)$. The project lifetime followed a discrete uniform range $N \sim \mathrm{Unif}\{20, \ldots, 30\}$, while degradation was modeled as $d \sim \mathrm{Tri}(0.4\%, 0.8\%, 1.2\%)$. A multiplier represented capital cost uncertainty. $\sim \mathrm{Tri}(0.75, 1.00, 1.25)$, and the OPEX rate as $\sim \mathrm{Tri}(1.5\%, 2.0\%, 3.0\%)$. The AI/controls cost premium was varied as $\sim \mathrm{Tri}(20, 35, 60)$ USD/m^2. Soiling-loss assumptions were also varied using Table 8 ranges, with S2 modeled as $\mathrm{Tri}(4\%, 8\%, 12\%)$ and S3 as $\mathrm{Tri}(4.5\%, 6\%, 7.5\%)$. These variations were applied by scaling annual energy yields relative to base-case values.

Two probability-based performance indicators are reported in Table 22. The first is the probability that S3 achieves a lower LCOE than S2, expressed as $P(\mathrm{LCOE}_{S3} < \mathrm{LCOE}_{S2})$. The second is the probability that the present value of the additional electricity generated by S3 exceeds the AI/controls cost premium, expressed as $P(\mathrm{PV}(\Delta E) > \mathrm{AI\ premium})$, consistent with the break-even framework in Table 15. For comparison, the same break-even probability is also reported for the maintenance-constrained case (S3b).

Table 22: Monte Carlo probabilities of S3 (and S3b) favorability relative to S2 (50,000 trials per site)

Site	$P(\mathrm{LCOE}_{S3} < \mathrm{LCOE}_{S2})$	$P(\mathrm{PV}(\Delta E_{S3-S2}) > \mathrm{AI\ premium})$	$P(\mathrm{PV}(\Delta E_{S3b-S2}) > \mathrm{AI\ premium})$
AlUla	64.5%	91.5%	29.7%
NEOM	61.1%	88.9%	25.2%
Red Sea	63.1%	89.3%	25.5%
Riyadh	57.4%	84.5%	19.4%

As shown in Table 22, S3 remains more cost-effective than S2 in most cases when evaluated using LCOE, with probabilities ranging from 57.4% to 64.5%. This indicates that uncertainty in factors such as AI cost and achievable soiling-loss reduction can sometimes reduce the advantage of S3. However, when evaluated using the break-even criterion based on the value of recovered electricity, S3 performs more strongly, with favorable outcomes in 84.5% to 91.5% of simulations, which is consistent with the deterministic findings in Table 15.

In contrast, Table 22 also shows that the maintenance-constrained scenario (S3b) has much lower probabilities of meeting the break-even condition, ranging from 19.4% to 29.7%. This demonstrates that limitations in executing maintenance actions significantly reduce the likelihood that the additional electricity generated can justify the AI/controls cost. Overall, these results confirm that S3 feasibility depends not only on average performance improvements but also on uncertainties in electricity value, discount rate, AI cost, and achievable soiling-loss reduction, while S3b provides a conservative lower-bound case under constrained maintenance conditions.

4.6. Synthesis for Saudi smart-city deployment

4.6.1. Site suitability insights and decision rules

Results were consistent across sites: S1 achieved the highest energy output and best economics; S2 showed a significant performance drop; and S3 reliably improved façade performance relative to S2, with an energy yield gain of ~8.75%–9.22%. Therefore, S3 reduced LCOE and shortened payback compared with S2, making it the stronger façade option when façades are part of the design.

S1 should be the default choice wherever roofs or dedicated PV areas are available, as it consistently outperforms transparent façades across yield and cost metrics. However, transparent façade PV remains useful as an added layer when roof PV is constrained by urban form or when daylighting and architectural value are priorities. In these cases, S3 should be chosen over S2 when maintenance access allows the condition-based actions to be executed in practice; otherwise, S3b provides a more realistic lower-bound estimate of the achievable uplift under façade-access constraints, while still improving performance relative to S2.

S3 is most justified when operational losses are expected to be significant or difficult to manage, especially when façade access constraints are maintenance-related. A practical procurement rule is to adopt S3 only when the discounted value of the extra electricity from the S3–S2 uplift exceeds the added controls/AI cost under the project's tariff and discount rate assumptions. As a result, a hybrid district strategy is recommended: deploy S1 for bulk, low-cost supply on roofs/fields, and use S3 on façades to add urban generation and strengthen visibility and ESG reporting per m^2 of envelope. Where façade access limits cleaning frequency or delays work-order execution, feasibility screening should use S3b (maintenance-constrained) performance as the conservative basis for procurement decisions, or include robotic/drone cleaning options if frequent condition-based cleaning is required.

Site signals aligned with this logic. AlUla presented the strongest case for S3, with the best yield and economics and the largest uplift, followed by NEOM, with high yield and strong financial results. The Red Sea site supported S3 but required strict monitoring and maintenance planning, while Riyadh showed the weakest performance and smallest uplift, meaning S3 should be used selectively there when façade value or roof constraints clearly justify it.

4.6.2. Planning implications for smart-city stakeholders

Façade teams can justify transparent BIPV when transparency, daylighting, or iconic design is essential; however, planning for S3-ready integration—monitoring routes, access, and maintainability—helps achieve expected yield and CO_2 reduction goals. Energy planners should treat S3 façades as a predictable, incremental resource that improves façade yield and reduces CO_2 by about 9% compared to S2, while still relying on S1 for most least-cost electricity.

For developers and investors, S3 consistently improved feasibility relative to S2 by lowering LCOE (~7.4%–7.9%) and shortening payback (~8.1%–8.8%); therefore, adoption depends on whether the value of recovered energy under project financial assumptions outweighs the added controls' cost. O&M teams should focus on soiling control and thermal-loss awareness as primary drivers of delivered kWh, while continuous monitoring and condition-based action reduce the risk of long, hidden losses on hard-to-access façades.

5. Discussion

This study examined how transparent building-integrated PV (BIPV) façades performed across representative Saudi smart-city locations in terms of energy output, cost, and carbon benefits. It also measured how adding an automated analytics-and-control layer changed results compared with a transparent façade run without that layer. Rather than re-establishing the well-known transparency–efficiency trade-off, the discussion focuses on what can be recovered operationally—i.e., the portion of the performance gap attributable to avoidable losses (particularly soiling and maintenance delays) that can be reduced through monitoring, decision rules, and timely interventions. Consistent with prior work, transparent PV output remains constrained by the light–power compromise: higher visible-light transmission leaves less usable irradiance for electricity generation, which explains why S2 and S3 produce lower annual energy than conventional PV (S1) even when operations improve (Huang and Markides, 2021; Katepalli et al., 2023).

Across all sites, transparent façades generated less electricity than conventional PV, which matches the wider literature showing that transparent devices often prioritize appearance and daylighting over conversion efficiency (Gupta et al., 2021). However, the enhanced-operation case delivered a consistent gain of about 9% compared with the transparent case without it, indicating that a measurable share of the annual shortfall is operational rather than purely material-limited. In this study, the AI-enabled layer is interpreted as an operational decision-support mechanism (performance estimation, deviation detection, event screening, and condition-based action) that primarily targets loss recovery rather than changing device physics. This aligns with broader research indicating that data-driven operations can improve renewable energy systems by enabling better planning, earlier fault detection, and more timely maintenance, especially under changing or harsh conditions (Abisoye et al., 2024; Arévalo and Jurado, 2024; Bennagi et al., 2024). Accordingly, the main contribution is the cross-site quantification of this recoverable component under a consistent per-m^2 façade functional unit, alongside decision-relevant implications for feasibility under harsh-climate losses and practical maintenance constraints. When façade access limits cleaning frequency or delays work-order execution, the realized benefit of AI-enabled operation may be closer to the maintenance-constrained case (S3b) than to the fully responsive case (S3). Accordingly, S3 results should be interpreted as an achievable target under timely condition-based interventions, whereas S3b provides a conservative lower-bound estimate of the operational uplift when high-rise maintenance logistics constrain response intervals.

In addition, the relatively small variation in uplift between locations implies that the modeled operating improvements—reducing losses and acting sooner—held up across different Saudi settings. Conceptually, this makes sense because such methods primarily reduce controllable or partially controllable losses, such as preventable downtime, suboptimal operating settings, and slow maintenance response times. Therefore, they improve delivered output without altering the fundamental efficiency ceiling set by the transparent PV layer itself (Boza and Evgeniou, 2021). This interpretation is consistent with the explicit AI workflow described in Section 3.4 (inputs → clean-power estimator → soiling indicator → threshold/persistence + event screening → feasible action scheduling), which frames AI as operational logic rather than a change in PV conversion physics.

From an investment standpoint, transparent façades (S2) did not match conventional PV (S1) in terms of cost per unit of electricity, as expected when energy yield falls but integration and balance-of-system costs remain substantial. This challenge is widely reported for BIPV and other advanced PV products, and the chosen boundaries and assumptions often influence it in the economic analysis (Chen et al., 2021). Even so, the added operational layer improved feasibility in the right direction: compared with S2, it lowered LCOE and shortened payback, despite adding a cost for the digital layer. The main reason was simple: higher lifetime kWh reduced LCOE, while the extra cost changed total lifetime cost by a smaller proportion. As a result, operational gains can create outsized economic benefits when limited energy production is the main bottleneck (Chen et al., 2021). However, the maintenance-constrained economics (S3b) demonstrate that this benefit is conditional: when cleaning execution is delayed or limited, the recovered kWh (and thus the economic improvement) shrinks, and the break-even margin relative to the AI/controls premium can narrow substantially.

The findings also align with a practical purchasing perspective tied to how new technologies evolve: as supporting tools mature, their added cost can decline while their operational value remains, improving affordability over time (Elia et al., 2021). This matters for Saudi smart-city programs because adoption choices are often made across a portfolio of options. Conventional PV typically remains the lowest-cost supply choice, while façade PV may still be selected for design, land-use, or district-planning reasons, provided its added cost per delivered kWh and per avoided CO_2 is acceptable (Al-Saidi, 2022; Islam and Ali, 2024). Importantly, the combined "economic realism" cases (joint variation of electricity value and discount rate) show that while S3 remains directionally better than S2, absolute attractiveness can weaken under conservative financing and tariff/value conditions, extending payback and reducing ROI; therefore, the feasibility claim should be interpreted as conditional rather than universal.

Setting operational CO_2 benefits to scale directly with delivered electricity yielded two key takeaways. First, the performance uplift translated almost directly into additional avoided CO_2 when a fixed grid emission factor was used, making carbon reporting straightforward and repeatable for operational accounting (Chenic et al., 2022). Second, the avoided CO_2 levels depended strongly on the chosen emission factor and, therefore, on how quickly the wider power system is decarbonizing. This dependence is expected when focusing only on operational impacts, and it aligns with how many energy-system studies frame decarbonization pathways.

To address the limitation of operational-only accounting for building-integrated systems, the study also reports a simplified embodied-CO_2 screening and a net CO_2 benefit indicator (operational avoided CO_2 minus annualized embodied CO_2). This screening-level extension does not replace a full ISO life-cycle assessment, but it provides a decision-support check on whether operational displacement remains positive after accounting for major façade-material and electronics contributions. Under the screening assumptions, net CO_2 remains positive across sites and transparent-façade cases, and the ranking follows delivered electricity (S3 > S3b > S2), reinforcing that operational yield recovery translates into both higher operational avoided CO_2 and improved net benefit when embodied burdens are annualized over the project lifetime.

The sensitivity analysis added practical insight by showing that LCOE and payback responded most to installed cost and to harsh-climate loss drivers, especially soiling losses and, to a lesser extent, heat-related output reduction. This ordering aligns with PV challenges in dusty regions and underscores the importance of anti-soiling measures, cleaning logistics, and ongoing performance checks (Al-Shetwi, 2022; Cherupurakal et al., 2021). For CO_2 outcomes, the grid emission factor had the strongest influence, underscoring that operational carbon results depend partly on the power system, not solely on PV technology. Complementing the OFAT results, the Monte Carlo uncertainty analysis provides a likelihood-based view: under joint parameter uncertainty, S3 remains favorable relative to S2 in a majority of trials, but feasibility likelihood decreases when AI premium increases, electricity value decreases, discounting increases, or realized loss-recovery is constrained (as represented by S3b).

A further implication is that the value of automated decision support should be judged alongside operational and maintenance practicality. When monitoring and guidance are improved, the risk of prolonged underperformance—caused by hard-to-access maintenance or unnoticed degradation—can be reduced, particularly in high-rise smart-city districts. As a result, this system-level view aligns with smart-city energy management work that emphasizes connected sensing, analysis, and operations rather than focusing solely on the device (Ali et al., 2023; Kim et al., 2021). In addition, the strengthened literature-based validation (including a façade-relevant benchmark for loss magnitude) increases confidence that the modeled derating mechanisms are plausible for vertical BIPV exposure, while still recognizing that monitored façade-scale datasets are required for full empirical validation.

For planners, the results point toward a mixed approach: use conventional PV (S1) as the main energy source where it can be installed easily, and use transparent façades with enhanced operation (S3) as a supporting resource in dense districts where building form and design constraints make façades attractive. This direction aligns with smart-city sustainability frameworks that consider multiple goals—energy, carbon, function, and governance—rather than optimizing a single measure (Almihat et al., 2022; Deeb et al., 2024). For designers and developers, the decision rule is also straightforward: S3 is the better choice than S2 when the extra recovered electricity is worth more than the added digital cost under the project's tariff and financing assumptions, and when limited access makes condition-based action especially valuable (Chen et al., 2021). Where façade access constraints are expected to delay or limit cleaning execution, feasibility screening should adopt the conservative S3b case (or comparable access-constrained assumptions), and economic realism conditions should be checked explicitly because high discounting and low electricity value can tighten or eliminate the break-even margin.

Finally, the study used simulation-based performance estimates and modeled operating losses, so the absolute KPI values still depend on assumptions such as soiling levels, cleaning effectiveness, tariffs, and emission factors. More generally, data quality and local specificity remain common constraints in data-driven energy operations, especially when methods are transferred across climates, sensor configurations, and operating practices (Abisoye et al., 2024; Bennagi et al., 2024). Therefore, on-site validation at façade scale—particularly for soiling behavior and maintenance access—would improve confidence in wider use. In addition, extending the environmental scope to full life-cycle boundaries would allow clearer comparison against embodied-carbon trade-offs in façade construction systems (Al-Shetwi, 2022; Chenic et al., 2022). While the embodied-carbon component reported here improves completeness relative to operational-only reporting, it remains a simplified screening; future work should refine component inventories, supplier-specific factors, and replacement modeling to strengthen net CO_2 comparisons for procurement-grade decisions.

6. Conclusions

This study evaluated transparent BIPV façades at representative locations in Saudi smart cities using three cases: conventional PV, transparent PV without AI, and AI-enabled transparent PV. Across all sites, conventional PV repeatedly produced the highest energy output and the best technical and financial results. Therefore, when rooftops or dedicated PV areas are available, it remains the most cost-effective option for delivering electricity.

Transparent façade PV without AI showed a noticeable drop in performance compared with conventional PV, and this lower output led to weaker results when costs were measured against electricity produced. As a result, transparent BIPV façades are better framed as an added layer of urban electricity generation that makes sense when façades must be used for architectural goals, daylight access, or land-use limitations, rather than as a one-to-one replacement for conventional PV.

Adding AI improved transparent façade performance compared with the transparent baseline without AI and delivered steady gains across sites in energy delivery, key technical and financial indicators, and operational avoided CO_2. These results suggest that some of the underperformance of transparent façades can be reduced through stronger monitoring, better operation informed by forecasts, and clearer maintenance decision support. However, the fundamental limit created by the transparency–efficiency trade-off remains. In addition, S3 results represent an achievable target under responsive maintenance; S3b represents a conservative case under façade-access constraints that may delay or limit condition-based interventions. Accordingly, the magnitude of realized uplift should be interpreted as conditional on the feasibility of executing condition-based actions (especially cleaning) at façade height.

The sensitivity analysis found that the strength of the economic case depended mainly on installed cost assumptions and harsh-climate loss factors, especially losses linked to soiling. Meanwhile, operational avoided the assumed grid emission factor strongly shaped the CO_2 results. Therefore, whether deployment is feasible depends not only on the chosen technology but also on realistic operations and maintenance planning and clear reporting of the financial and emissions assumptions used. Under the combined economic realism cases (joint variation of electricity value and discount rate), S3 remains directionally better than S2, but absolute attractiveness weakens as electricity value decreases and discounting increases; thus, payback/ROI thresholds for adoption should be evaluated under project-specific tariff and financing conditions rather than assumed to hold universally. Monte Carlo uncertainty results further reinforce this point by quantifying that S3 is favorable relative to S2 in a majority of trials under defined uncertainty ranges, while feasibility likelihood declines when AI premium is higher, electricity value is lower, discounting is higher, or maintenance execution is constrained (as represented by S3b).

Overall, the findings support a mixed smart-city approach: prioritize conventional PV for most energy supply and use, and deploy AI-enabled, transparent façades that provide added functional value and whose extra operational benefits are sufficient to justify the added system complexity. In practical high-rise applications, procurement and feasibility screening should interpret S3 as the best-case outcome under timely maintenance execution and use S3b as a lower-bound estimate when façade access limits cleaning frequency or delays work-order completion. From an environmental-reporting perspective, operational avoided CO_2 remains useful for near-term displacement accounting; however, the addition of an embodied-CO_2 screening and net CO_2 indicator provides a more complete interpretation for BIPV, and net-benefit conclusions should reference this screening-level adjustment when embodied impacts are material. Future work should focus on real-world façade-scale validation, a better understanding of soiling, and the practicality of maintenance at height, and on expanding environmental assessment beyond operational boundaries when reporting frameworks require it. Future work should also refine embodied inventories (supplier-specific factors and replacement modeling) and extend probabilistic analyses as additional monitored façade datasets become available to constrain uncertainty for procurement-grade decisions better.

List of abbreviations

AC	Alternating current

AI	Artificial intelligence
BAPV	Building-applied photovoltaics
BIPV	Building-integrated photovoltaics
CAPEX	Capital expenditure
CI	Cleaning interval
DC	Direct current
DHI	Diffuse horizontal irradiance
DNI	Direct normal irradiance
EF	Emission factor
ESG	Environmental, social, and governance
GHI	Global horizontal irradiance
IGU	Insulated glazing unit
ISO	International Organization for Standardization
KPI	Key performance indicator
LCA	Life-cycle assessment
LCOE	Levelized cost of electricity
NOCT	Nominal operating cell temperature
O&M	Operation and maintenance
OFAT	One-factor-at-a-time
OPEX	Operating expenditure
POA	Plane-of-array irradiance
PR	Performance ratio
PV	Photovoltaic(s)
ROI	Return on investment
SD	Standard deviation
STC	Standard test conditions
TMY	Typical meteorological year
TPV	Transparent photovoltaic
UV	Ultraviolet
VLT	Visible light transmittance

Acknowledgment

The authors gratefully acknowledge the support of the Faculty of Civil Engineering, Department of Environmental Engineering, Universiti Teknologi Malaysia (UTM), in facilitating this research. The authors also acknowledge Qatar University for institutional support. Any opinions, findings, and conclusions expressed in this paper were those of the authors and did not necessarily reflect the views of the supporting institutions.

Compliance with ethical standards

Conflict of interest

The author(s) declared no potential conflicts of interest with respect to the research, authorship, and/or publication of this article.

References

Abisoye BO, Sun Y, and Zenghui W (2024). A survey of artificial intelligence methods for renewable energy forecasting: Methodologies and insights. Renewable Energy Focus, 48: 100529. https://doi.org/10.1016/j.ref.2023.100529

Al Garni HZ (2022). The impact of soiling on PV module performance in Saudi Arabia. Energies, 15(21): 8033. https://doi.org/10.3390/en15218033

Alafnan H (2024). Sustainable cities: The economic feasibility of 50% renewable energy production for the city of Ha'il in Saudi Arabia. In the 2024 IEEE 8th Energy Conference (ENERGYCON), IEEE, Doha, Qatar: 1-6. https://doi.org/10.1109/ENERGYCON58629.2024.10488791

Alazazmeh A, Ahmed A, Siddiqui M, and Asif M (2022). Real-time data-based performance analysis of a large-scale building applied PV system. Energy Reports, 8: 15408-15420. https://doi.org/10.1016/j.egyr.2022.11.057

Ali SA, Elsaid SA, Ateya AA, ElAffendi M, and El-Latif AAA (2023). Enabling technologies for next-generation smart cities: A comprehensive review and research directions. Future Internet, 15(12): 398. https://doi.org/10.3390/fi15120398

Almihat MGM, Kahn MTE, Aboalez K, and Almaktoof AM (2022). Energy and sustainable development in smart cities: An overview. Smart Cities, 5(4): 1389-1408. https://doi.org/10.3390/smartcities5040071

Al-Saidi M (2022). Energy transition in Saudi Arabia: Giant leap or necessary adjustment for a large carbon economy? Energy Reports, 8: 312-318. https://doi.org/10.1016/j.egyr.2022.01.015

Al-Shetwi AQ (2022). Sustainable development of renewable energy integrated power sector: Trends, environmental impacts, and recent challenges. Science of the Total Environment, 822: 153645. https://doi.org/10.1016/j.scitotenv.2022.153645 **PMid:35124039**

Ang TZ, Salem M, Kamarol M, Das HS, Nazari MA, and Prabaharan N (2022). A comprehensive study of renewable energy sources: Classifications, challenges and suggestions. Energy Strategy Reviews, 43: 100939. https://doi.org/10.1016/j.esr.2022.100939

Antonanzas J, Osorio N, Escobar R, Urraca R, Martinez-de-Pison FJ, and Antonanzas-Torres F (2016). Review of photovoltaic power forecasting. Solar Energy, 136: 78-111. https://doi.org/10.1016/j.solener.2016.06.069

Arévalo P and Jurado F (2024). Impact of artificial intelligence on the planning and operation of distributed energy systems in smart grids. Energies, 17(17): 4501. https://doi.org/10.3390/en17174501

Ashraf M, Ayaz M, Khan M, Adil SF, Farooq W, Ullah N, and Nawaz Tahir M (2023). Recent trends in sustainable solar energy conversion technologies: Mechanisms, prospects, and challenges. Energy & Fuels, 37(9): 6283-6301. https://doi.org/10.1021/acs.energyfuels.2c04077

Baras A, Jones RK, Alqahtani A, and Alodan M (2016). Measured soiling loss and its economic impact for PV plants in central Saudi Arabia. In the 2016 Saudi Arabia Smart Grid (SASG), IEEE, Jeddah, Saudi Arabia: 1-7. https://doi.org/10.1109/SASG.2016.7849657

Bennagi A, AlHousrya O, Cotfas DT, and Cotfas PA (2024). Comprehensive study of the artificial intelligence applied in renewable energy. Energy Strategy Reviews, 54: 101446. https://doi.org/10.1016/j.esr.2024.101446

Boza P and Evgeniou T (2021). Artificial intelligence to support the integration of variable renewable energy sources to the power system. Applied Energy, 290: 116754. https://doi.org/10.1016/j.apenergy.2021.116754

Chen C, Hu Y, Karuppiah M, and Kumar PM (2021). Artificial intelligence on economic evaluation of energy efficiency and renewable energy technologies. Sustainable Energy Technologies and Assessments, 47: 101358. https://doi.org/10.1016/j.seta.2021.101358

Chenic AȘ, Cretu AI, Burlacu A, Moroianu N, Vîrjan D, Huru D, Stanef-Puica MR, and Enachescu V (2022). Logical analysis on the strategy for a sustainable transition of the world to green energy—2050. Smart cities and villages coupled to renewable energy sources with low carbon footprint. Sustainability, 14(14): 8622. https://doi.org/10.3390/su14148622

Cherupurakal N, Mozumder MS, Mourad AHI, and Lalwani S (2021). Recent advances in superhydrophobic polymers for antireflective self-cleaning solar panels. Renewable and Sustainable Energy Reviews, 151: 111538. https://doi.org/10.1016/j.rser.2021.111538

Deceglie MG, Micheli L, and Muller M (2018). Quantifying soiling loss directly from PV yield. IEEE Journal of Photovoltaics, 8(2): 547-551. https://doi.org/10.1109/JPHOTOV.2017.2784682

Deeb YI, Alqahtani FK, and Bin Mahmoud AA (2024). Developing a comprehensive smart city rating system: Case of Riyadh, Saudi Arabia. Journal of Urban Planning and Development, 150(2): 04024012. https://doi.org/10.1061/JUPDDM.UPENG-4707

Elia A, Kamidelivand M, Rogan F, and Gallachóir BÓ (2021). Impacts of innovation on renewable energy technology cost reductions. Renewable and Sustainable Energy Reviews, 138: 110488. https://doi.org/10.1016/j.rser.2020.110488

Gupta M, Dubey AK, Kumar V, and Mehta DS (2021). Experimental study of combined transparent solar panel and large Fresnel lens concentrator based hybrid PV/thermal sunlight harvesting system. Energy for Sustainable Development, 63: 33-40. https://doi.org/10.1016/j.esd.2021.05.008

Hoang AT and Nguyen XP (2021). Integrating renewable sources into energy system for smart city as a sagacious strategy towards clean and sustainable process. Journal of Cleaner Production, 305: 127161. https://doi.org/10.1016/j.jclepro.2021.127161

Huang G and Markides CN (2021). Spectral-splitting hybrid PV-thermal (PV-T) solar collectors employing semi-transparent solar cells as optical filters. Energy Conversion and Management, 248: 114776. https://doi.org/10.1016/j.enconman.2021.114776

Islam MT and Ali A (2024). Sustainable green energy transition in Saudi Arabia: Characterizing policy framework, interrelations and future research directions. Next Energy, 5: 100161. https://doi.org/10.1016/j.nxener.2024.100161

Izam NSMN, Itam Z, Sing WL, and Syamsir A (2022). Sustainable development perspectives of solar energy technologies with focus on solar photovoltaic—A review. Energies, 15(8): 2790. https://doi.org/10.3390/en15082790

Kalimeris A, Psarros I, Giannopoulos G, Terrovitis M, Papastefanatos G, and Kotsis G (2023). Data-driven soiling detection in PV modules. IEEE Journal of Photovoltaics, 13(3): 461-466. https://doi.org/10.1109/JPHOTOV.2023.3243719

Katepalli A, Wang Y, and Shi D (2023). Solar harvesting through multiple semi-transparent cadmium telluride solar panels for collective energy generation. Solar Energy, 264: 112047. https://doi.org/10.1016/j.solener.2023.112047

Kim H, Choi H, Kang H, An J, Yeom S, and Hong T (2021). A systematic review of the smart energy conservation system: From smart homes to sustainable smart cities. Renewable and Sustainable Energy Reviews, 140: 110755. https://doi.org/10.1016/j.rser.2021.110755

Konstantinou C (2021). Toward a secure and resilient all-renewable energy grid for smart cities. IEEE Consumer Electronics Magazine, 11(1): 33-41. https://doi.org/10.1109/MCE.2021.3055492

Mohamed I, Diab MR, Elbatran AA, and Abdelmotalib HM (2026). Performance assessment of building-integrated photovoltaic facade system in harsh climate: A case study in Aswan. Results in Engineering, 30: 110475. https://doi.org/10.1016/j.rineng.2026.110475

Sepúlveda-Oviedo EH, Travé-Massuyès L, Subias A, Pavlov M, and Alonso C (2023). Fault diagnosis of photovoltaic systems using artificial intelligence: A bibliometric approach. Heliyon, 9(11): e21491. https://doi.org/10.1016/j.heliyon.2023.e21491 **PMid:37954345 PMCid:PMC10637999**

Wolniak R and Stecuła K (2024). Artificial intelligence in smart cities—applications, barriers, and future directions: A review. Smart Cities, 7(3): 1346-1389. https://doi.org/10.3390/smartcities7030057

Zhang L, Ling J, and Lin M (2022). Artificial intelligence in renewable energy: A comprehensive bibliometric analysis. Energy Reports, 8: 14072-14088. https://doi.org/10.1016/j.egyr.2022.10.347